Neutronic Design and Analysis of the Holos-Quad Concept

Progress of Holos ARPA-E project from ANL design team

Nuclear Science and Engineering Division

About Argonne National Laboratory

Argonne is a U.S. Department of Energy laboratory managed by UChicago Argonne, LLC under contract DE-AC02-06CH11357. The Laboratory's main facility is outside Chicago, at 9700 South Cass Avenue, Argonne, Illinois 60439. For information about Argonne and its pioneering science and technology programs, see www.anl.gov.

Neutronic Design and Analysis of the Holos-Quad Concept

Progress of Holos ARPA-E project from ANL design team

prepared by
N. Stauff, C. Lee, P. Shriwise, Y. Miao, R. Hu, P. Vegendla, T. Fei
Nuclear Science and Engineering Division, Argonne National Laboratory

June 5, 2019

EXECUTIVE ABSTRACT

HolosGen, LLC is proposing a highly innovative micro-reactor concept targeting both civilian and military applications. It consists of an advanced helium-cooled gas reactor using a turbojet-type turbine and compressor to achieve a highly condensed reactor that fits into a commercial ISO container. The Holos-Quad concept being considered for civilian applications will generate 22MWt, using four Subcritical Power Modules (SPMs) that fit into one 40-foot ISO container. It is a high-temperature gas-cooled reactor concept using TRISO fuel distributed in graphite hexagonal blocks, cooled with helium gas at 7MPa and a high outlet temperature.

In FY2019, HolosGen, LLC received an ARPA-E MEITNER grant to team up with the Argonne National Laboratory (ANL) design team to demonstrate the feasibility of the Holos-Quad concept in terms of neutronics. In particular, the evaluation study of the Holos design features and alternative options for reactivity control was considered. Through these tasks, the ANL design team has been working on demonstrating the feasibility of the Holos-Quad concept in terms of neutronics to help advance the core design of the Holos-Quad.

A rigorous design approach was employed for the Holos-Quad in order to ensure that the input space is fully investigated, and that the best solutions are considered. The first step of this approach consisted of properly defining the Holos-Quad design problem by identifying the competitive design objectives: its economic performance is maximized with longer lifetime and its transportability to remote locations is maximized with reduced weight. The design problem also required to identify the operational constraints (in terms of thermal hydraulics, reactivity feedback and shutdown margins) and the input parameters that could be varied.

In the second step, a sensitivity analysis was performed to enable preliminary investigation of the input space to identify the correlations among input and output variables. It allowed, for instance, to find input parameters that have relatively poor impact on the core performance and that could be removed from the optimization problem to accelerate its convergence. This sensitivity analysis showed that the design problem defined is highly constrained since only 117 solutions out of 1,000 simulated cores met all the design constraints.

The design optimization was performed in the third step employing a genetic algorithm to effectively explore this highly constrained input space and find global optimal solutions. More than 2,500 cores were fully evaluated to converge to a Pareto Frontier of optimum solutions providing best compromise between the life-time target and the total core weight, as shown in Figure 1. The main benefit of this approach was to reduce the human effort and to be able to automatically re-run the optimization problem when changing the design problem. The multi-objective optimization identified various core solutions that would be optimum solutions for different types of applications.
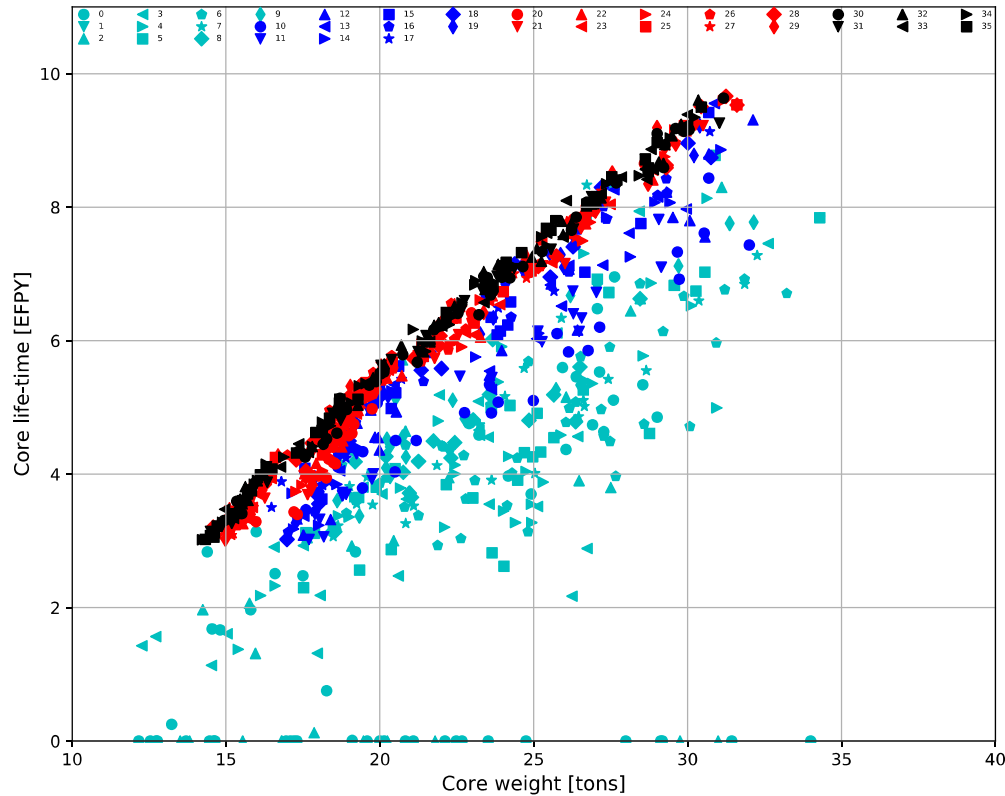
Figure 1. Pareto Frontier obtained from the multi-criteria optimization.

For applications where economics matters less while the focus is on the ease of transportation, a core weight of ~15 tons can achieve lifetime of ~3.5 EFPY. For applications where economics matters the most and ease of transportation matters less, a lifetime of 8.3 EFPY can be achieved with a total core weight of ~26.7 tons. This latter design was determined to be the best configuration that would meet the design requirements of the ARPA-E project and was further investigated with detailed analyses.

In order to give confidence in the neutronic models employed and in the core performance obtained, a detailed neutronic benchmark was proposed based on the selected optimum Holos-Quad core concept. Engineers at ANL within the Nuclear Science and Engineering (NSE) Division and the Mathematical Computer and Science (MCS) Division performed independent neutronic evaluations using different Monte Carlo codes (SERPENT and OpenMC) and the PROTEUS deterministic code. The results obtained showed good agreement in the many different evaluated parameters on a unit cell problem and on the full core problem and confirmed the performance of the optimum Holos-Quad concept. Detailed neutronic and thermal-hydraulics were then performed on the optimum core selection in order to provide more details on the power and temperature distributions, to assess the impact from modeling assumptions, and to evaluate alternative design options. Finally, a very preliminary investigation of secondary control system and shutdown margins was provided.

Shielding analyses were performed by the ARPA-E resource team, and preliminary results are summarized in this report to complete the neutronic feasibility demonstration of this concept.

The shielding requirement was assessed for the turbomachinery equipment in the ISO container, which is located near the core. Preliminary results showed that it is important to include ~5cm side shield to prevent the streaming neutrons from reaching the turbine and limit its dose below 0.1 DPA. Another shielding analysis focused on the personnel dose rate outside the reactor building, and the thickness of the building wall outside the ISO container was determined from a parametric study. Finally, the shielding requirements during transportation of a single irradiated SPM in an ISO container was evaluated. Preliminary estimation showed 20cm lead shield surrounding the fuel cartridge would be sufficient to satisfy the dose rate limit around the ISO container.

To conclude, the ANL team performed a wide range of extensive analyses in FY2019 to demonstrate the neutronic feasibility of the Holos-Quad micro-reactor concept by proposing an optimum design of the core, thoroughly analyzing it, and performing preliminary shielding analyses. On all these tasks, extensive work is still required to improve some of the economics and neutronics performance. The focus of additional core design optimization will be on reducing the excess reactivity by employing alternative burnable poisons and on investigating different secondary control systems. A detailed evaluation of shutdown margins for both primary and secondary control systems that include uncertainties and reactivity faults will be completed. Finally, the Holos-Quad design optimization will be updated to include several design improvements to improve core performance, which should help avoiding potential reactivity insertion during flooding scenarios in transportation. Those scenarios will be further evaluated through the core design optimization process.

Finally, the experience and methods developed at ANL in this project for VHTR-types micro-reactor analyses could be directly applicable to advance the design and analyses of additional Holos concepts that are developed for other applications, such as the Titan concept for higher power output and better economic performance, or the SCO FOAK for improved transportability.

Table of Contents

LIST OF FIGURES

LIST OF TABLES

1 Introduction

Micro nuclear reactors are being developed for different applications such as deployment in harsh locations, long term electricity supply to a remote area, emergency power to a natural disaster location, etc. [1] For easy and quick deployment to locations where the external power grid and operation personal are limited, a very small reactor not only in power rate but also in physical size is favorable. A power rate less than 20MWe and factory manufacturing are preferred, together with a high level of passive safety and an autonomous reactor control system.

HolosGen, LLC (HolosGen) is proposing a highly innovative micro-reactor concept targeting both civilian and military applications. It consists of an advanced helium-cooled gas reactor using a turbojet-type turbine and compressor to achieve a highly condensed reactor that fits into a commercial ISO container. The Holos-Quad concept being considered for civilian applications will generate 22MWt, using four Subcritical Power Modules (SPMs) that fit into one 40-foot ISO container. It is a high-temperature gas-cooled reactor concept using TRISO fuel distributed in Graphite hexagonal blocks, cooled with Helium gas at 7MPa and a high outlet temperature (650°C is being used in this report, but higher temperatures are being considered as well).

In FY2019, HolosGen received an ARPA-E MEITNER grant to team up with the Argonne National Laboratory (ANL) design team to demonstrate the feasibility of the Holos-Quad concept in terms of neutronics, and help advance the core design of the Holos-Quad. In particular, the evaluation study of the Holos design features and alternative options for reactivity control was considered. Through these tasks, the innovative Holos design features will be demonstrated and preferred core design parameters will be determined allowing to move forward with the successful completion of the Holos core development.

This report discusses the progress made by the ANL design team in the first part of FY2019. After a brief description of the codes and models employed in Section 2, the method developed for core design is described in Section 3. The best core design is selected to perform a neutronic benchmark described in Section 4 in order to confirm modeling capabilities. Detailed neutronic and thermal-hydraulics analyses performed on the optimum core selection are described in Section 5. Section 6 summarizes the preliminary shielding analysis performed by the resource team of ARPA-E. Finally, the conclusions of this study are discussed in Section 7.

2 Codes Employed

2.1 SERPENT

The Monte Carlo code SERPENT [2] is the main code employed for neutronic simulations for core design and analysis in this work. It is a continuous-energy Monte-Carlo reactor physics burnup calculation code developed at the VTT Technical Research Center of Finland. In this analysis, SERPENT is used for detailed core modeling, employing the ENDF/B-VII.1 nuclear data library.

The fuel region is modeled with an explicit description of the TRISO fuel where particles are distributed with semi-random sampling technique; they are filled in a compact regular lattice, and random particles are then removed to meet the packing fraction requested.

For the burnup depletion calculation, the full core is being depleted using a unique depletion region in the core optimization and neutronic benchmark analysis. The impact of this approximation is addressed in Section 5.3.

2.2 OpenMC

OpenMC [3] is being applied in analysis of the Holos-Quad concept as a tool for verification of the neutronics benchmark calculations being performed with SERPENT. OpenMC is an open-source Monte Carlo code originally developed at the Massachusetts Institute of Technology in 2011. Various institutions, laboratories, and organizations now contribute to the development of OpenMC.

OpenMC is capable of continuous energy neutron and photon transport with support for TRISO modeling along with analogous physics models to those found in SERPENT. An identical TRISO fuel particle distribution to the one used in SERPENT is applied in all OpenMC models in this report. All geometry, materials, and depletion zones in SERPENT calculations are matched in the OpenMC model as well.

2.3 PROTEUS

The PROTEUS code [4] is a high-fidelity capable three-dimensional (3D) deterministic neutron transport code developed by ANL under the Department of Energy (DOE) Nuclear Energy Advanced Modeling and Simulation (NEAMS) program. Being able to solve the neutron transport equation in steady-state and transient conditions, the code contains three solvers for flexible applications: the second-order discrete ordinates (SN) and method of characteristics (MOC) transport solvers based on unstructured finite element meshes as well as the nodal transport solver (NODAL) for hexagonal and Cartesian geometries for use in rapid design application. The SN and MOC solvers are based on 3D meshes and 2D extruded meshes, respectively, to solve 3D neutron transport problems. Multigroup cross sections for the code can be generated using MC2-3 or Monte Carlo codes (SERPENT or OpenMC) externally, or on-the-fly using the cross section API inside the code. Geometry and meshes are generated using CUBIT for non-standard geometry problems or the in-house mesh toolkit developed by ANL for standard, typical Cartesian and hexagonal type, geometry problems.

In this work, the Holos-Quad was modeled using the MOC transport solver with explicit geometry. Four input files are required for PROTEUS calculations, which include files for geometry and mesh, cross sections, mapping between geometry and material, and calculation

options. For geometry and mesh, the CUBIT mesh generation software was first used since the geometry of Holos cores are non-standard. Since it is not trivial to generate geometry and mesh for such a complex-geometry core, we used CUBIT to generate the geometries and meshes for core components which were merged using the in-house mesh toolkit to construct a whole core. Since PROTEUS-MOC was used, a 2D geometry and mesh was prepared with the meshing tools, assuming an extruded mesh, and a 3D core was constructed by assigning materials in the axial direction at the input file for mapping between geometry and material. For multigroup cross sections, the 14-group cross sections based on the group structure were generated using SERPENT. More details on the model developed with PROTEUS is provided in Appendix B.

2.4 DAKOTA

The DAKOTA software [5] maintained by Sandia National Laboratory is an uncertainty quantification and optimization toolkit with over 20 years of supporting development. DAKOTA provides advanced mathematical methods to vary one code's input parameters and analyze the output results, enabling multi-objective optimization and uncertainty quantification analysis. DAKOTA was integrated in the NEAMS Workbench [6] for improved user experience and to facilitate coupling with any other application as performed in Section 3.2.

2.5 SAM

The System Analysis Module (SAM) [7] is a modern system analysis tool under development at ANL for advanced non-LWR safety analysis. It aims to provide fast-running, whole-plant transient analyses capability with improved-fidelity. SAM takes advantage of advances in physical modeling, numerical methods, and software engineering, to enhance its user experience and usability. It is a system-level modeling and simulation tool with higher fidelity but yet computationally efficient. The initial SAM development focus was on liquid cooled reactors, but more recently, SAM is being supported under DOE and NRC to model HTGR technology. SAM leverages modern advanced software environments and numerical methods, and is well suited to be further developed as a key tool for High Temperature Gas-cooled Reactor (HTGR) modeling and simulation at the reactor plant scale and for reactor safety analysis.

The HolosGen fuel assembly consists of multiple coolant channels and heat structures such as fuel, graphite, lead-buffer and cladding (as shown in Figure 3-2). The SAM PBCoreChannel component was used to model both coolant channel (1D) and heat structures (2D), with the axis-symmetric configuration shown in Figure 2-1. The fuel assembly is modeled by a representative pin-cell, which represents an average fuel pin, graphite, buffer, clad, and coolant channel (the dimensions of the model are re-computed for each core design considered). To develop the SAM model, the required information for this component includes heat structure thickness, coolant channel hydraulic diameter, total coolant channel cross section area, length of the core, heat surface area density, power distribution and number of fuel rods.

In the SAM model, a homogenized assumption was applied for the fuel region, although the fuel was compacted with the TRISO particles. To obtain the kernel temperature of TRISO particles, the analytical temperature distribution of the spherical geometry was applied using the fuel temperature.
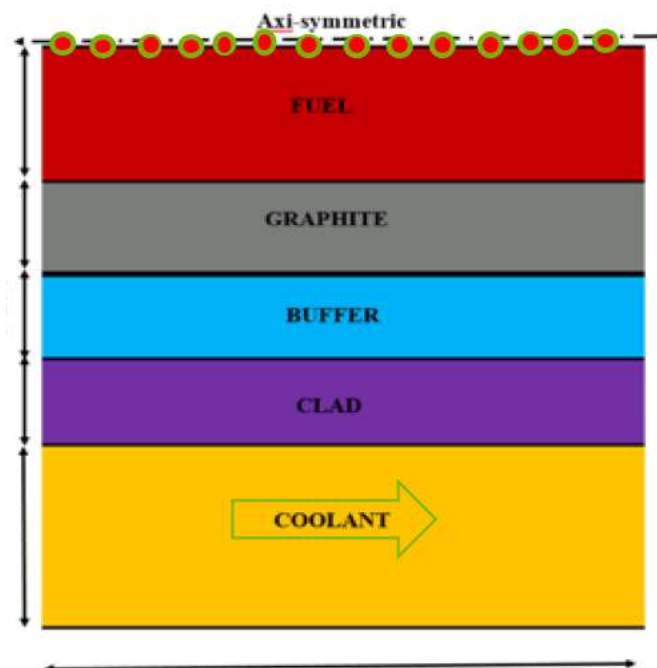
Figure 2-1. 2D model of the coolant channel considered.

3 Core Design Optimization

The main objective of the design team collaboration between ANL and HolosGen is to demonstrate feasibility of Holos-Quad concept with attractive core performance. For this, the core design approach developed in [8] was applied to this project. This multi-step procedure enables one to properly formulate the design problem, ensure the input space is being fully investigated, and that the best solutions are being considered for any potential applications of the Holos-Quad concept. The first step of the design approach consists of properly defining the design problem (step 1). This step is followed by sensitivity analysis (step 2) and multi-criteria analysis (step 3). The optimum core design selected will undergo detailed neutronic analyses in Section 4 and Section 5.

3.1 Step 1: Definition of the Core Design Problem

The first step of a core design consists of properly defining the design problem, which means determining performance parameters to optimize the input variables and the design constraints needed to be considered.

3.1.1   Holos-Quad core Design Problem Introduction

The Holos-Quad is a high-temperature gas-cooled reactor (HTGR) concept generating 22MWt designed to fully fit into one 40-foot ISO container and to be transported through traditional means of transportation (truck, plane, boat, helicopter, etc.). The available width and height of the ISO container is limited to 2.34 m, as shown in Figure 3-1. The length of the 40-foot ISO container (12 m) does not constrain the core design of the Holos-Quad.

The Holos-Quad is formed by four independent subcritical power modules (SPMs) enabling power generation when a minimum number of SPMs are actively positioned by actuators to satisfy criticality requirements. Each SPM contains its own closed-loop, gas Brayton cycle with a turbine, compressor, inter-cooler, etc., generating 5.5MW thermal power. Currently, only one reactivity control system is being considered: the capability to manage reactivity by moving SPMs apart and increasing the neutron leakage. A secondary control system is being developed in a secondary stage, as initiated in Section 5.6. Additional emergency shutdown system, which will also be used for transportation, considers addition of a Hafnium blade between the four SPMs.

For improved inherent safety, the Holos-Quad uses TRISO particle fuel distributed in graphite hexagonal blocks. To remain in the range of readily available material technology, the coolant temperature was limited to 650°C, but higher temperatures are being considered for the next stage of this project to enhance thermal efficiency of the Brayton cycle.

Each SPM is wrapped inside a shell of zircaloy-4. The purpose of the shell is mainly to avoid air interacting with graphite. Its purpose is not structural and it will not be subjected to excessive stress. The core weight will be held via structural components in the coolant sleeves and a solid structure outside the fuel cartridge. In addition, its temperature will be limited by the use of thermal insulator material (such as a layer of porous carbon). Additional structural material analysis will be needed in the future to confirm the feasibility of this concept.
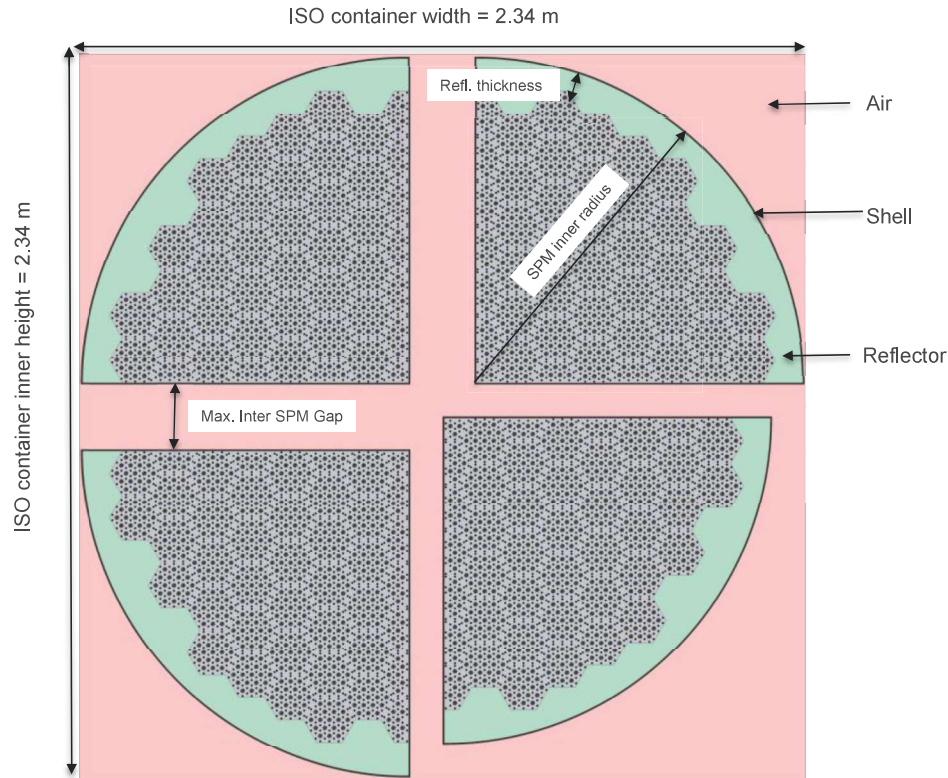
Figure 3-1. Transversal core layout.

In order to limit the pressure on the shell (and its thickness), the pressurized He coolant is contained inside the coolant channels, as shown in the assembly description on Figure 3-2 and Figure 3-3. Currently, those are also made of zircaloy. For high temperature applications, SiC with Nb liner will be considered in the future.

For neutronics modeling consideration, three core configurations are considered with following changes in cross-section temperatures. At this stage of our study, changes in density (from thermal expansion) were not considered, and all dimensions provided are at **hot temperature** conditions. In the future, better definition of the shutdown states should be provided.

- Full power: Fuel temp = 900K, Coolant+Structure = 800K

- Hot shutdown: Fuel temp = 800K, Coolant+Structure = 800K

- Cold shutdown: Fuel temp = 300K, Coolant+Structure = 300K

Here is a non-exhaustive list of simplifications and assumptions that will be resolved during the next stage of this project by the ARPA-E design and resource teams at ANL and HolosGen:

- Currently, the graphite and beryllium blocks used in the fuel and reflector assemblies are supposed to be perfectly cut to fit into the cylindrical shell (see Figure 3-1).

- No cooling material channel is currently considered in the radial reflector block. However, coolant channels are considered in the axial reflectors.

- The channels containing the flow of cold coolant returning to the compressor were not modelled. It is envisioned to be located in a cavity located between the radial reflector and the outside shell (whose shape will not be cylindrical anymore to accommodate additional volume).
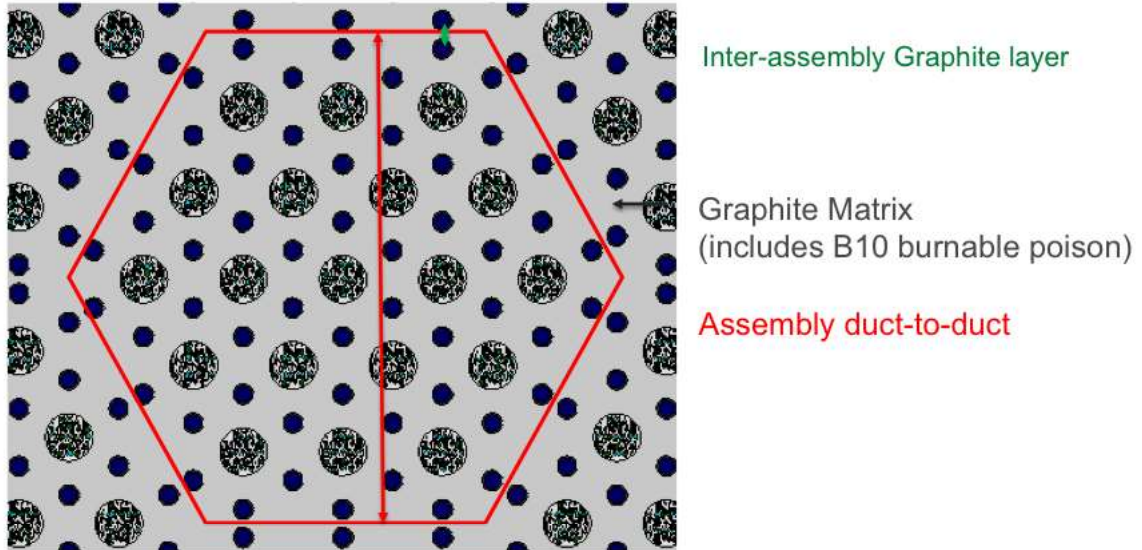
Figure 3-2. Assembly layout for Holos-Quad.
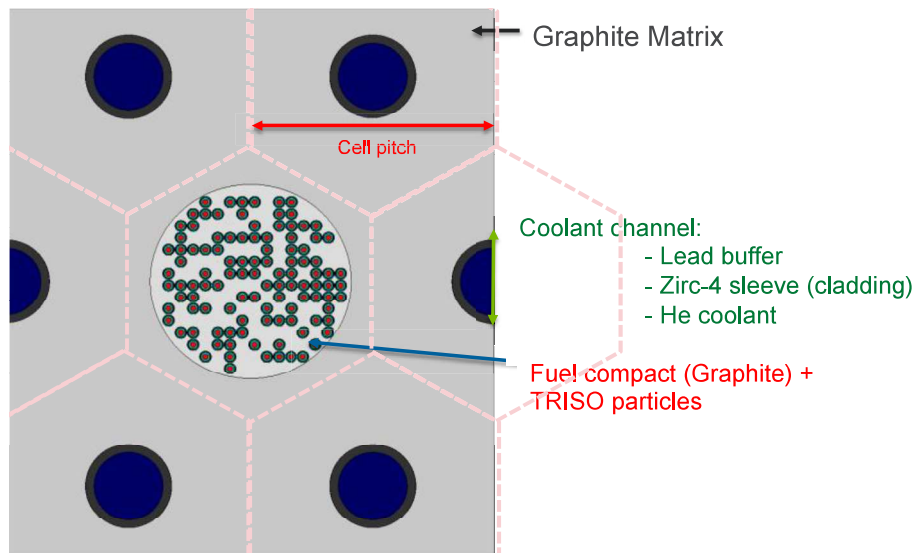
Figure 3-3. Cell layout for Holos-Quad.

3.1.2 Optimization Goals

Upon discussion with HolosGen, it was determined that the Holos-Quad parameters to be optimized are the core life-time and weight. Both of these competing metrics try to maximize two important aspects of the Holos-Quad concept: its economic performance and its transportability.

a. Core Life-Time

The Holos-Quad is targeting long life-time in order to improve the economics of the system by enabling continuous operations for several years after installation. In this report, the core life-time is defined as the **full power** irradiation time over which the core maintains the effective multiplication factor (k-eff) larger than 1.02. The limit of 1.02 was decided to maintain operational flexibility even at End Of Life (EOL) and compensate for xenon poisoning, as discussed in Section 5.4. Consequently, this metric is a conservative value of the total irradiation life-time that would also need to consider increased life-time due to load following operation, and potential life-time extension with reduced flexibility and reduced core power.

b. Core Weight

The total core weight of the Holos-Quad should be limited in order to facilitate means of transportation to remote location by helicopter or airplane. The core weight is estimated as the total weight of material in the core, considering:

- The driver fuel regions: containing the weight of the TRISO particles, of the graphite, of the coolant channels made of helium coolant, zircaloy-4 cladding, and lead buffer.

- The axial and radial reflector regions. Beryllium metal was selected for its low weight and excellent reflector performance, despite its lower melting temperature and its toxicity. The impact of using beryllium metal versus graphite of beryllium oxide is discussed in Section 5.5.

- The shell material structure, which is currently also made of zircaloy-4.

For every material considered in this work, the weight density in the neutronic model and in the weight calculation is provided in Appendix A: MASS Densities of Materials Considered. The other structural components (turbine, coolers, etc.) are not considered in this neutronic optimization since they will not be affected by the design choices considered here.

3.1.3 Design Constraints

The design constraints for the Holos-Quad concept are separated into 3 different sub-constraints:

- Reactivity shutdown: those simplified constraints consider the capability to shut down the core at any time of the irradiation. They account for potential increase in the k-eff value during irradiation due to the use of burnable poisons, and for statistical uncertainty of the Monte Carlo solution. Two constraints are considered:

  1. CSD : Reactivity at cold shutdown < 0.95, considering maximum separation of the 4 SPMs with insertion of 1cm thick Hafnium blade using Equation (1).

$$Max\left(k_{eff}^{CSD}\right) = Max\left(k_{eff}(t)\right) - k_{eff}(0) + k_{eff}^{CSD}(0) + \frac{\sigma(k_{eff}(0))}{2} < 0.95 \qquad (1)$$

  2. HSD: Reactivity at hot shutdown < 0.98, considering maximum separation of only 3 out of 4 SPMs to model the impact of failure to move one SPM using Equation (2).

$$Max\left(k_{eff}^{HSD}\right) = Max\left(k_{eff}(t)\right) - k_{eff}(0) + k_{eff}^{HSD}(0) + \frac{\sigma(k_{eff}(0))}{2} < 0.98 \qquad (2)$$

- Reactivity feedback constraints are evaluated at Beginning Of Life (BOL) where the MDC is more constraining due to the presence of burnable poisons diluted in the graphite moderator.

3. Moderator Density Coefficient (MDC) < 0, calculated by reducing the graphite density of the fuel pin matrix and the graphite block by 1% (density of Be reflector is not changed) and accounting for statistical uncertainty with Equation (3)

$$10^5 * \left(\frac{1}{k_{eff}^{Ref}(0)} - \frac{1}{k_{eff}^{MDC}(0)} + \frac{\sqrt{\sigma(k_{eff}^{Ref}(0))^2 + \sigma(k_{eff}^{MDC}(0))^2}}{2} \right) < 0 \qquad (3)$$

4. Fuel Temperature Coefficient < 0, calculated by increasing the temperature of the UCO fuel by 300K (from 900K to 1200K) and accounting for statistical uncertainty with Equation (4).

$$10^5 * \left(\frac{1}{k_{eff}^{Ref}(0)} - \frac{1}{k_{eff}^{FTC}(0)} + \frac{\sqrt{\sigma(k_{eff}^{Ref}(0))^2 + \sigma(k_{eff}^{FTC}(0))^2}}{2} \right) < 0 \qquad (4)$$

- Thermal hydraulics constraints are estimated with SAM on the hot channel, considering radial power peaking of 1.5868, and axial power peaking of 1.1821. Both power peaking values were evaluated with PROTEUS on an early version of the Holos-Quad design and should be relatively realistic values for the first round of design optimization study performed in this report.

5. Peak Pressure Drop < 3 bars
6. Nominal Peak TRISO Temperature < 1250°C

- Flooding constraint: An additional reactivity shutdown constraint that needs to be considered is the capability to remain sub-critical in cold shutdown state during flooding event with water around the SPMs and inside the coolant channels. The water brings additional reactivity is this potentially under-moderated reactor (since graphite is not as good a moderator as water). This scenario is evaluated but not currently used as a hard constraint in this optimization problem since doing so requires design of secondary control system that will bring additional shutdown margins. It will be added as a hard constraint in the next round of optimization.

3.1.4 Input Parameters

The list of design parameters that were fixed, varied, and evaluated as a function of the varied parameters is listed in Table 3-1. For the varied parameters, the upper, lower bonds and the number of points within this range used in the optimization are listed in Table 3-2. As discussed in Reference [8], the convergence of the optimization calculation is improved if performed on discrete variables instead of continuous ones.

Table 3-1. Design parameters used for modeling the Holos-Quad core (hot conditions).

	Parameters	Unit	Value
Container	Inner height/width modeled	m	2.34/2.34
Shell	Thickness	cm	0.50
	Material		Zirc-4
	Inner radius	m	*evaluated*
Core	Power	MWt	22
	Total Number of fuel columns		***varied***
	Height of the fuel column	m	***varied***
	Height of upper/lower reflector	m	***varied***
	Thickness of radial reflector	cm	***varied***
	Fuel form		UCO C/U=0.4 O/U=1.5
Fuel block	Pitch	cm	*evaluated*
	Number of fuel holes		19
	Number of small coolant holes		54
Fuel cell	Pitch of fuel cell	cm	***varied***
	Radius of fuel hole	cm	0.70
	Diameter of fuel compact	cm	0.0855
	Packing fraction	%	***varied***
	Outside radius of coolant hole	cm	***varied***
	Coolant cladding	Material	Zirc-4
	Coolant cladding thickness	cm	0.057
	Lead buffer thickness (between coolant cladding and graphite)	μm	20
	Inside radius of coolant hole	cm	*evaluated*
Particle size	Kernel diameter		425
	Buffer thickness		100
	Inner pyrolytic carbon thickness	μm	40
	Silicon carbide thickness		35
	Outer pyrolytic carbon thickness		40
Material density	Fuel kernel (UCO)		10.744
	Buffer		1.04
	Inner pyrolytic carbon		1.882
	Silicon carbide (SiC)		3.171
	Outer pyrolytic carbon		1.882
	Graphite block (matrix)	g/cm^3	1.806
	Be block (reflector)		1.778
	Coolant He		0.00365
	Air (inter-modules – N$_2$)		0.0012
	Lead		10.2530
	Zircaloy-4 (SPM shell)		6.489
Uranium enrichment		at.%	19.95
B10 Burnable absorbent material		ppm	***varied***

Table 3-2. Variable input design parameters.

Design parameter	Variable Name	Lower bound	Upper bound	Num. points
Height of the driver fuel	H	200 cm	500 cm	31
Height of Axial reflector	h	5 cm	25 cm	5
TRISO packing fraction	PF	25%	40%	2
Number of Assemblies	NA	151	249	10
Thickness of radial reflector (estimate of the thickness of reflector between the fuel block furthest away from the center, and the shell)	Tr	5 cm	15 cm *(constrained by geometry)*	11
Cell pitch	p	1.4 cm	1.75 cm	8
Inter-assembly graphite layer	It	0.05 cm	0.4 cm	8
Coolant hole radius	r_c	0.30	0.38	6
Burnable poison concentration (average, only in graphite block – not in pin)	BP	10 ppm	25 ppm	13

3.1.5 Summary

The Holos-Quad core design problem defined in this Section is summarized in Figure 3-4. For this ARPA-E project, the minimum core life-time targeted was arbitrarily set to 8 years in order to favor the techno-economic analysis. As a consequence, the objective of the core design work proposed in this report is to find the smallest and lightest core configuration that meets this lifetime objective together with all the design constraints.

Constraints:
- Shutdown k-eff < 0.95
- Reactivity control k-eff < 0.98
- Moderator density coefficient < 0
- Fuel temp. coefficient < 0
- TRISO temp < 1250 °C
- Pressure drop < 3 bars

Design parameters to optimize:
- Number of assemblies
- Height of the driver fuel
- Height of axial reflector
- Thickness of radial reflector
- TRISO packing fraction
- Cell pitch
- Inter-assembly graphite layer
- Coolant hole radius
- Burnable poison conc.

Objective functions:
+ Core lifetime (**k-eff > 1.02**)
- Core weight

Figure 3-4. Description of the optimization problem.

3.2 Method Developed for Holos Core Design

Solving the core optimization problem described in Section 3.1.5 can be done through a manual sensitivity analysis, which requires good understanding of the physics and testing of many design configurations. However, to save user time and ensure systematic investigation of the input space, it was decided to employ a formal mathematical optimization approach that had been recently developed [8] and applied to sodium-cooled fast reactor (SFR) core design.

The full input space considered with the parameters listed in Table 3-2 contains 150 million options. An efficient optimization algorithm is able to navigate this input space efficiently to converge to the best options within limited runs. Still, the main challenge of such approach is to be relatively computationally expensive since ~2,500 cores will be modeled in Section 3.4 to reach acceptable convergence. However, the main benefit of this approach is the reduced human effort (after the initial setup of the problem) and to be able to automatically re-run the optimization problem when changing the design problem (adding input parameters, relaxing constraints, etc.).

The PyHolos software introduced in Figure 3-5 was developed to take the templated input with design information and to generate, execute and post-process simultaneous SAM and SERPENT calculations to simulate the steady-state performance of the core modeled (weight, core lifetime), its shutdown reactivity margins, etc. The PyHolos code enables efficient and quality-controlled simulations. It can be adapted with little effort to any changes in the Holos core design for instance to change the number of SPMs, location of the hafnium blade or of the alternative reactivity control systems, etc.
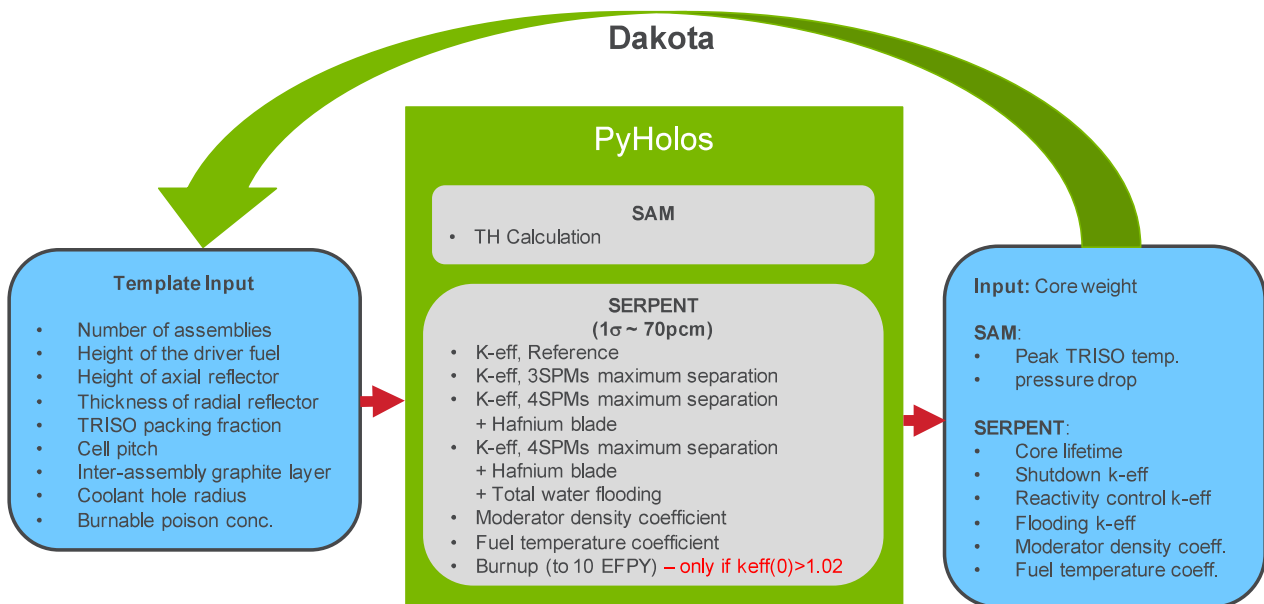
Figure 3-5. Overview of the PyHolos software framework for Holos-Quad optimization.

The main benefit of the PyHolos framework is to enable simple coupling with the DAKOTA code [5] through the NEAMS Workbench driver interface [6, 8], also shown in Figure 3-5. DAKOTA samples each input parameters with Latin Hypercube Sampling (LHS) technique and generates user-defined number of PyHolos inputs, which formulates the initial population. The Workbench

driver interface invokes the PyHolos code to execute each of the generated inputs, and extracts output responses of interest through individual runs of SAM and SERPENT. Multiple inputs can be executed at the same time at this step. Once the calculations of all inputs are finished, DAKOTA analyzes the extracted output responses. For core optimization analysis, DAKOTA employs a genetic algorithm to generate the inputs of the next generation. This iterative procedure continues until optimization convergence is achieved, with the final generation being the sets of optimal solutions.

3.3 Step 2: Sensitivity Analysis

Prior to running the full optimization problem (performed in Step 3), a global sensitivity analysis is suggested as the second step to investigate the correlations among core output variables, which represents the global trade-off among core optimization objectives. The sensitivity coefficients between inputs and outputs, which represent the impact of variation in input on the variation of output, should also be calculated in this step to identify the important core design parameters of the optimization problem. A few iterations can be expected between Step 1 and Step 2 to properly set up the core optimization problem.

The Latin Hypercube Sampling (LHS) technique implemented in DAKOTA was used to perform the sensitivity analysis. LHS is a stratified Monte Carlo sampling method which has good space-filling properties and the ability to induce a correlation structure across the sample variables. LHS is typically more efficient than Monte Carlo sampling, resulting in statistical estimators that have lower variance [9].

The results from the sensitivity analysis shown in Table 3-3 indicate that out of 1,000 simulated cores, only 117 meet all constraints while displaying a core lifetime larger than 0. All of the designs considered meet the thermal hydraulics constraints. However, 24% did not meet the reactivity feedback constraints due to positive MDC. Among those meeting the reactivity feedback constraints, only 30% met the reactivity shutdown constraints, mainly due to the inability to compensate the excess reactivity with sufficient margins at hot shutdown.

Table 3-3. Number of cores sampled meeting design constraints.

Number of samples *(LHS sampling)*	*All results* *1000*	*lifetime > 0* *721*
Meet thermal-hydraulics constraints	1000	721
Meet reactivity feedback constraints	765	589
Meet reactivity shutdown constraints	224	117

Each core sampled that met the design constraints listed in Section 3.1.3 is displayed with a point on Figure 3-6. This represents 224 points, with 117 that have core life-time > 0. This figure illustrates that each point represents a unique fully characterized core, and that long core life-time is achievable with larger core weight, confirming that these objective functions are competing against each other. The purpose of the optimization study proposed in Step 2 is to find the best possible compromise between both performance objectives.
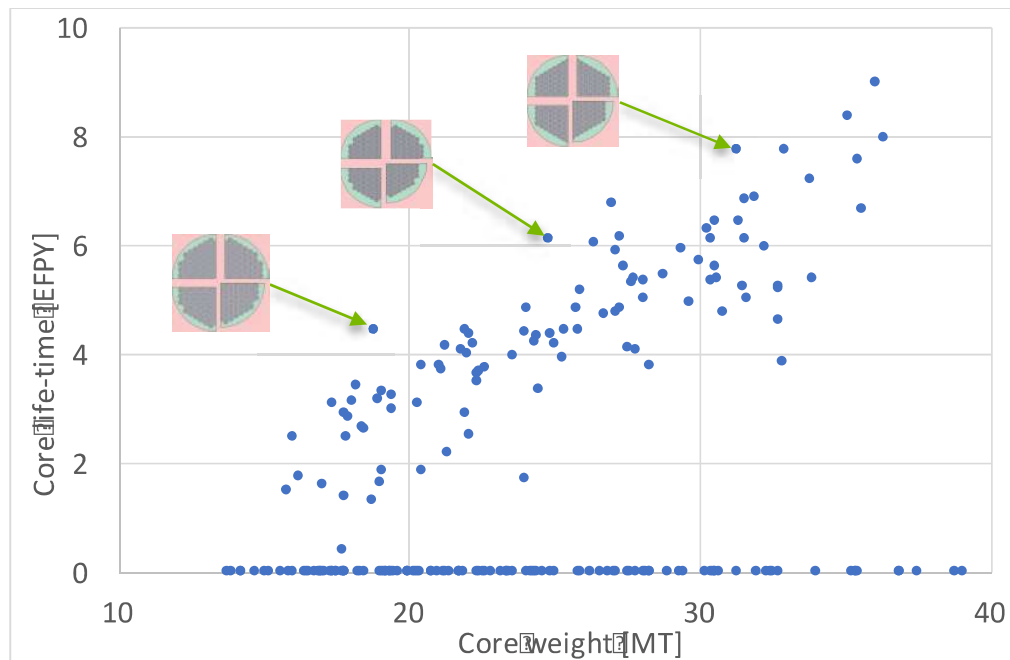
Figure 3-6. Performance of all the cores sampled meeting design constraints.

Finally, the results from the sensitivity analysis can be used to compute the Pearson correlation matrix within the different inputs and outputs of each simulation, as shown in Table 3-4. As expected, there is strong negative correlation between the number and length of the fuel cartridge, and the pressure drop and peak temperature in the TRISO fuel (i.e., more and longer coolant channels lead to reduced power density and flow rate, and reduced temperature and pressure drop). Such sensitivity analysis is especially useful to determine that parameters such as the axial reflector length and the inter-assembly graphite layer do not impact significantly the performance of the core and could be removed from the optimization problem to simplify it and to accelerate its convergence.

Table 3-4. Pearson correlations between Inputs and Outputs.

| | | Input Parameters | | | | | | | | | Optimization Goals | | Design Constraints | | | | | | |
		NA	H	h	lt	p	rc	BP	PF	Tr	Weight	Lifetime	Control	MDC	FTC	Shutdown	Flooding	Pressure Drop	TRISO Temp
Optimization Goal	Weight	0.2	0.9	0.2	0.0	0.2	0.0	0.0	0.0	0.1	1.0								
	Lifetime	0.0	0.4	0.1	0.0	0.1	-0.1	-0.5	0.4	0.1	0.5	1.0							
Design Constraints	Control Rod	0.3	0.2	0.1	0.1	0.4	-0.1	-0.4	0.2	0.3	0.4	0.6	1.0						
	MDC	-0.1	0.1	0.1	0.0	0.0	-0.1	0.3	-0.3	0.2	0.1	-0.2	0.0	1.0					
	FTC	-0.1	0.0	0.0	0.0	0.6	-0.1	-0.1	-0.6	0.1	0.1	-0.1	0.2	0.4	1.0				
	Shutdown	0.0	0.2	0.1	0.0	0.1	-0.3	-0.3	0.4	0.2	0.3	0.7	0.8	0.0	0.0	1.0			
	Flooding	0.1	0.1	0.0	0.0	-0.4	0.1	-0.5	0.7	0.0	0.1	0.6	0.4	-0.3	-0.5	0.7	1.0		
	Pressure Drop	-0.4	0.4	0.0	0.0	0.0	-0.7	0.0	0.0	0.0	0.3	0.3	0.0	0.2	0.1	0.3	-0.1	1.0	
	TRISO temp	-0.4	-0.9	0.0	0.0	0.0	0.1	0.0	-0.1	0.0	-0.9	-0.5	-0.3	0.0	0.1	-0.3	-0.2	-0.3	1.0

3.4 Step 3: Multi-Criteria Core Design Optimization

The main objective of the third step is to determine the best core options with minimum core weight at different targeted lifetimes, while meeting all the operational constraints. To solve this

multi-criteria optimization problem, a genetic algorithm was applied due to its capability to effectively explore a highly constrained input space to find global optimal solutions.

The results in Figure 3-7 show the evolution of the performance of the best set of 200 cores for each generation (35 generations were considered). The calculation was stopped at generation 35 (requiring a total of >2500 core simulations) when the performance improvements of the cores in the Pareto Front was found to be limited. The Pareto Front is a clustering of the optimum solutions. Core designs located in Pareto Frontier are optimal solutions suggested by the multi-objective optimization method, each of which reflects the trade-off among the two performance criteria considered in this design problem.
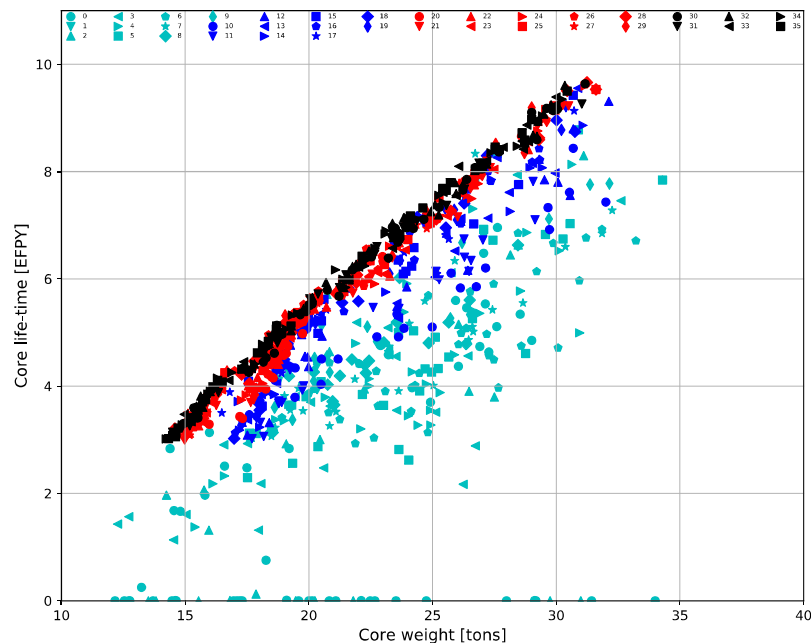
Figure 3-7. Pareto Frontier obtained from the multi-criteria optimization. Each generation of solution is shown with different shapes and color.

Figure 3-7 clearly illustrates the design compromise between the life-time target and the core weight required. Using current technologies and sets of constraints, the core lifetime of ~3.5 EFPY can be achieved with a total core weight of ~15 tons. If the core weight can be increased to 30 tons, the lifetime achievable is ~9 EFPY.

A few promising input solutions are displayed in Table 3-5 with increasing life-time achieved. As observed in this table, all the core concepts meet the design constraints. It is interesting to note that all the design options of the Pareto Front converged to the same number of fuel assembly (minimum number provided in the optimization problem), of packing fraction (maximum number provided in the optimization problem), and of coolant hole radius (minimum number provided in the optimization problem). Consequently, achieving better performance would be possible by extending the input space with reduced number of fuel assemblies and reduced coolant radius. However, such reduction will further increase the pressure drop, which is fine in terms of constraint, but may reduce the thermal efficiency of the Brayton cycle. This economic tradeoff was not considered at this time but should be in the future. To meet the lifetime objective of 8 years defined under the ARPA-E project for the Holos-Quad, the core concept "Opt 8" with a

total weight of ~26.7 tons was selected for neutronic benchmark in Section 4 and for additional detailed analysis in Section 5.

Table 3-5. Sample of optimum core solutions.

	Opt 3	Opt 4	Opt 5	Opt 6	Opt 7	**Opt 8**	Opt 9
Input variables							
Height of driver fuel [cm]	210	230	270	330	360	**390**	440
Height of Axial reflectors [cm]	5	5	5	5	5	**5**	5
Inter-assembly graphite layer [cm]	0.25	0.2	0.2	0.4	0.25	**0.25**	0.25
Cell pitch [cm]	1.65	1.7	1.7	1.65	1.7	**1.7**	1.7
External coolant hole radius [cm]	0.3	0.3	0.3	0.3	0.3	**0.3**	0.3
Burnable poison concentration [ppm]	10	13	16	16	10	**20**	11
TRISO packing fraction	0.4	0.4	0.4	0.4	0.4	**0.4**	0.4
Thickness of radial reflector [cm]	8	8	7	6	5	**7**	5
Number of Assemblies	151	151	151	151	151	**151**	151
Performance							
Core Weight [tons]	14.2	16.2	18.6	21.6	23.8	**26.7**	29.0
Lifetime [EFPY]	3.0	4.0	5.0	6.0	7.1	**8.3**	9.2
Constraints							
1- Control K-eff (CSD)	0.92	0.95	0.94	0.91	0.96	**0.97**	0.97
2- Shutdown K-eff (HSD)	0.83	0.84	0.83	0.81	0.84	**0.85**	0.85
3- MDC [pcm/%]	-234	-174	-188	-112	-167	**-120**	-105
4- FTC [pcm/300K]	-934	-862	-912	-848	-782	**-934**	-752
5- Peak pressure drop [bar]	0.36	0.39	0.46	0.56	0.61	**0.65**	0.74
6- Peak TRISO temp [Celcius]	989	967	935	902	889	**879**	865

4 Neutronic Benchmark Specifications and Results

The objective of the neutronic benchmark described in this section is to provide detailed description of the optimum Holos-Quad core concept selected for additional detailed analyses in Section 5. To demonstrate that the core performance of the Holos-Quad was properly estimated using SERPENT during the design optimization stage, a neutronic benchmark evaluation was proposed. Different engineers at ANL within the Nuclear Science and Engineering (NSE) Division and within the Mathematical Computer and Science (MCS) Division performed independent neutronic evaluations using different codes, the results of which are summarized in this Section.

4.1 Benchmark Specifications

4.1.1 Geometry Description

The Holos-Quad core model was built based on discussions with HolosGen and optimized using a genetic algorithm within DAKOTA, and the core parameters are summarized in

Table 4-1. The fuel assembly layout used is shown in Figure 4-1: it contains 19 fuel compacts, each being surrounded by 6 coolant channels. Helium is used as the coolant material. The packing fraction considered is 40% and the fuel uses high-essay low-enriched uranium with U-235 enrichment of 19.95 at%.

The transversal and horizontal layouts of the Holos reactor core are displayed in Figure 4-2 and Figure 4-3: it contains 151 fuel assemblies (some of which are axially and/or radially split) of 4.0m-long, which include 3.9m of fuel and 0.05m of upper and lower reflectors. The assembly "cut" is performed so that pins and coolant channels are not split, as shown in Figure 4-4. The total fuel inventory weight is 0.886 tons, which includes 0.809 ton of heavy nuclei.
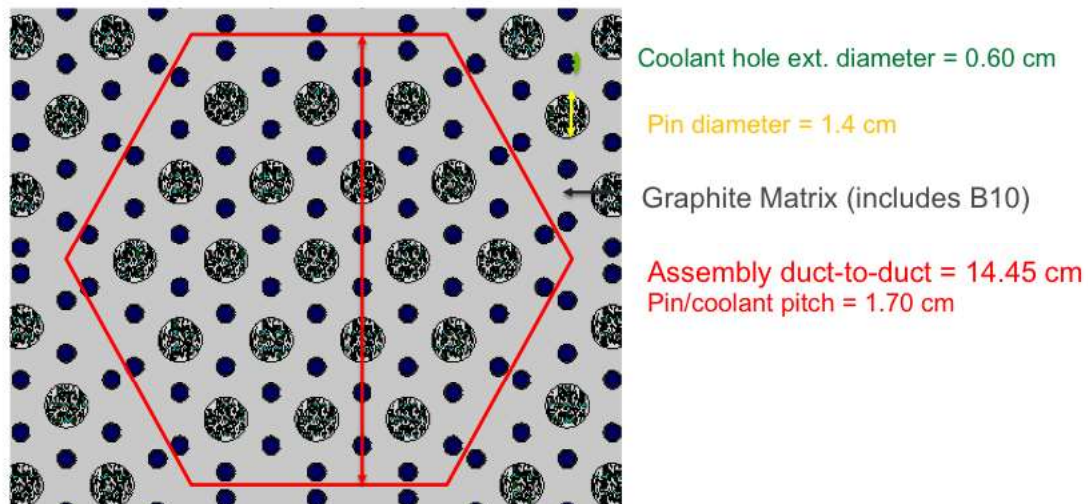
Figure 4-1. Assembly dimensions for Holos-Quad core.

Table 4-1. Design parameters used for modeling the Holos-Quad core (hot conditions).

	Parameters	Unit	Value
Container	Inner height/width modeled	m	2.34/2.34
Shell	Thickness	cm	0.50
	Material		Zirc-4
	Inner radius	m	1.045375
Core	Power	MWt	22
	Number of full fuel columns		132
	Number of half fuel columns		36
	Number of quarter fuel columns		4
	Height of the fuel column	m	3.90
	Height of upper/lower reflector	m	0.05
	Fuel form		UCO C/U=0.4 O/U=1.5
Fuel block	Pitch	cm	14.45
	Number of fuel holes		19
	Number of small coolant holes		54
Fuel cell	Pitch of fuel cell	cm	1.70
	Radius of fuel hole	cm	0.70
	Diameter of fuel compact	cm	0.0855
	Packing fraction	%	40
	Outside radius of coolant hole	cm	0.30
	Coolant cladding	Material	Zirc-4
	Coolant cladding thickness	cm	0.057
	Lead buffer thickness (between coolant cladding and graphite)	μm	20
	Inside radius of coolant hole	cm	0.241
Particle size	Kernel diameter	μm	425
	Buffer thickness		100
	Inner pyrolytic carbon thickness		40
	Silicon carbide thickness		35
	Outer pyrolytic carbon thickness		40
Material density	Fuel kernel (UCO)	g/cm^3	10.744
	Buffer		1.04
	Inner pyrolytic carbon		1.882
	Silicon carbide (SiC)		3.171
	Outer pyrolytic carbon		1.882
	Graphite block (matrix)		1.806
	Be block (reflector)		1.778
	Coolant He		0.00365
	Air (inter-modules – N$_2$)		0.0012
	Lead		10.2530
	Zircaloy-4 (SPM shell)		6.489
Uranium enrichment		at.%	19.95
B10 Burnable absorbent material (only in graphite block – not in pin)		ppm	20
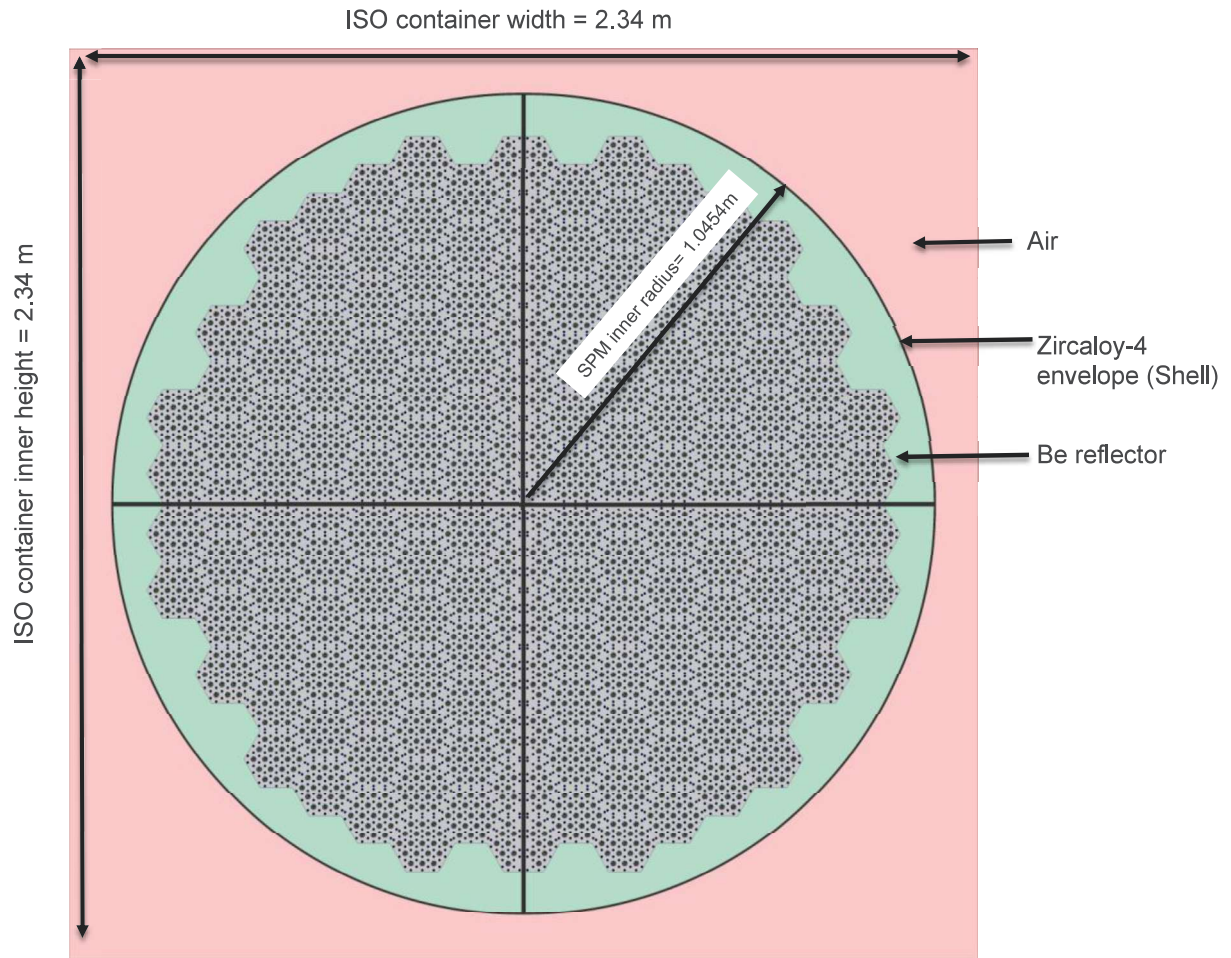
Figure 4-2. Transversal layout for Holos-Quad core.
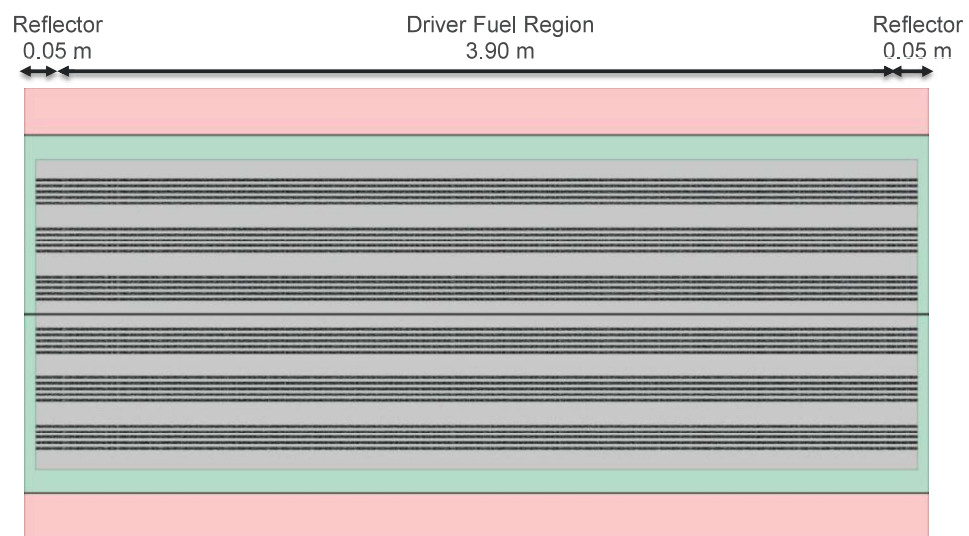
Figure 4-3. Horizontal layout for Holos-Quad core.
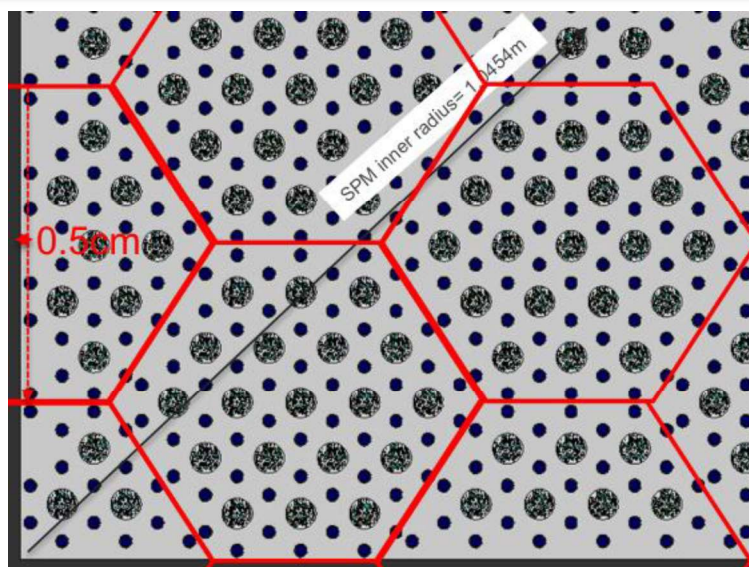
Figure 4-4. Zoomed-in image on the central region of one SPM.

4.1.2 Modeling Requirements

The following requirements were adopted for the different evaluations.

- A consistent nuclear data library should be employed based on MCNP-generated ENDF/B-VII.1
- The TRISO particle lattice should use same distribution.
- The temperatures for cross-sections of fuel, structure and coolant and for thermal scattering library must be consistent between different codes.
- For stochastic codes, computations should employ 500 active cycles with:
  o 10,000 particles for cell calculation and for depletion calculation on full core
  o 50,000 particles for full core k-eff
- Depletion calculations should use the time-steps requirements in Table 4-2.

Table 4-2. Depletion time steps.

Depletion days [EFPD]
0.3
2.0
36.5
365
730
1,095
1,460
1,825
2,737.5
3,650

4.1.3 Infinite Cell Benchmark Specifications

To make sure satisfactory agreement is reached without error cancellation, a simple unit-cell benchmark is proposed based on the model shown in Figure 4-5.
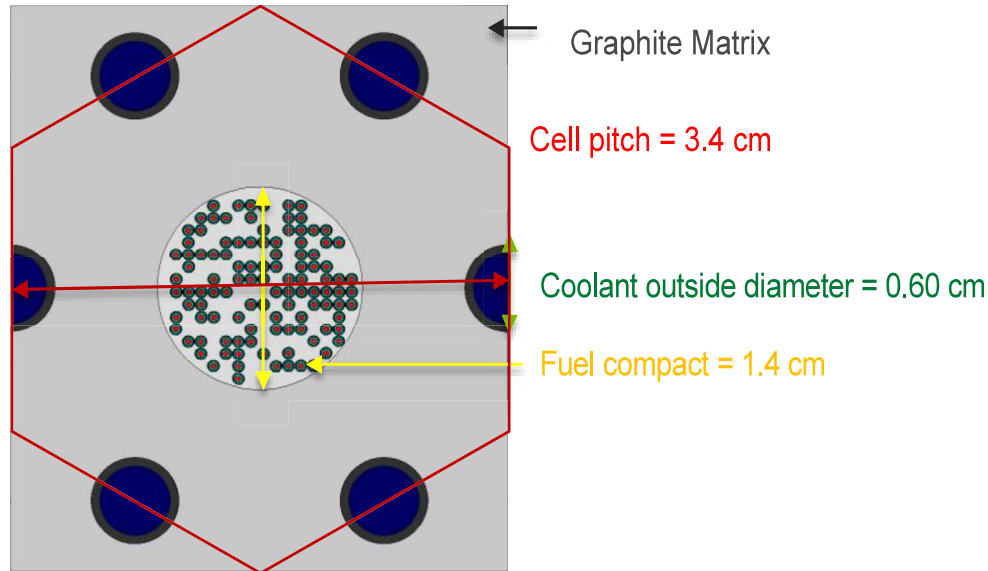
Figure 4-5. Infinite lattice cell model.

For this analysis, the following set of eigenvalue calculations were performed:

1. REF: Calculations with all cross-sections at 800K (including for thermal scattering libraries), except for fuel (UCO) at 900K.

2. Calculations with all cross-sections at 300K (including for thermal scattering libraries).

3. Calculations with all cross-sections at 800K (including for thermal scattering libraries) with Doppler broadening rejection correction for U-238 (only readily available with OpenMC).

4. Calculations with all cross-sections at 800K (including for thermal scattering libraries).

5. REF + no thermal scattering for Graphite.

6. REF + B-10 concentration in Graphite matrix set to 0.

7. Calculations with all cross-sections at 300K (including for thermal scattering libraries) + He coolant in graphite hole replaced with Water (density = 1.0 g/cm^3).

8. REF + graphite density reduced by 1% in block and pin.

9. REF + Depletion calculation which must include depletion of Graphite matrix region at time steps described in Table 4-2 with power of the cell of 7.868kW.

4.1.4   Full Core Benchmark Specifications

For the full-core analysis, the following set of eigenvalue calculations are requested, and the different core configurations are displayed on Table 4-3:

1. Reference K-eff

2. The reactivity worth of controlling SPM separation is assessed by moving 3 SPMs out of 4, with maximum gap thickness of 21cm. The fuel temperature is 800K (hot shutdown).

3. The shutdown margins are assessed with k-effective of Holos-Quad with maximum gap thickness between each of the 4 SPMs and insertion of Hafnium blade (1cm thick, 13.203g/cm^3). The fuel and structure temperatures are 300K (cold shutdown).

4. The water flooding scenario during shutdown configuration (described in #3) is assessed by modeling water (1g/cm^3, 300K) in coolant holes and outside SPMs. The fuel and structure temperature are 300K (cold shutdown).

5. The moderator density coefficient is calculated by reducing the graphite density of the fuel pin matrix and the graphite block by 1% (density of Be reflector is not changed).

6. The Doppler coefficient is calculated by increasing the temperature of the UCO fuel by 300K (to 1200K).

7. Depletion calculation that must include depletion of Graphite matrix region at burnup steps described in Table 4-2 with full core power of 22MWt.

Table 4-3. Holos-Quad core geometry with different SPM configurations.

| Reference (Calcs #1, 5, 6, 7) | 21cm gap, 3 SPMs moved (Calc #2) |
| 21cm gap, Hafnium blade (Calc #3) | 21cm gap, Hafnium blade, Total water flooding (Calc #4) |
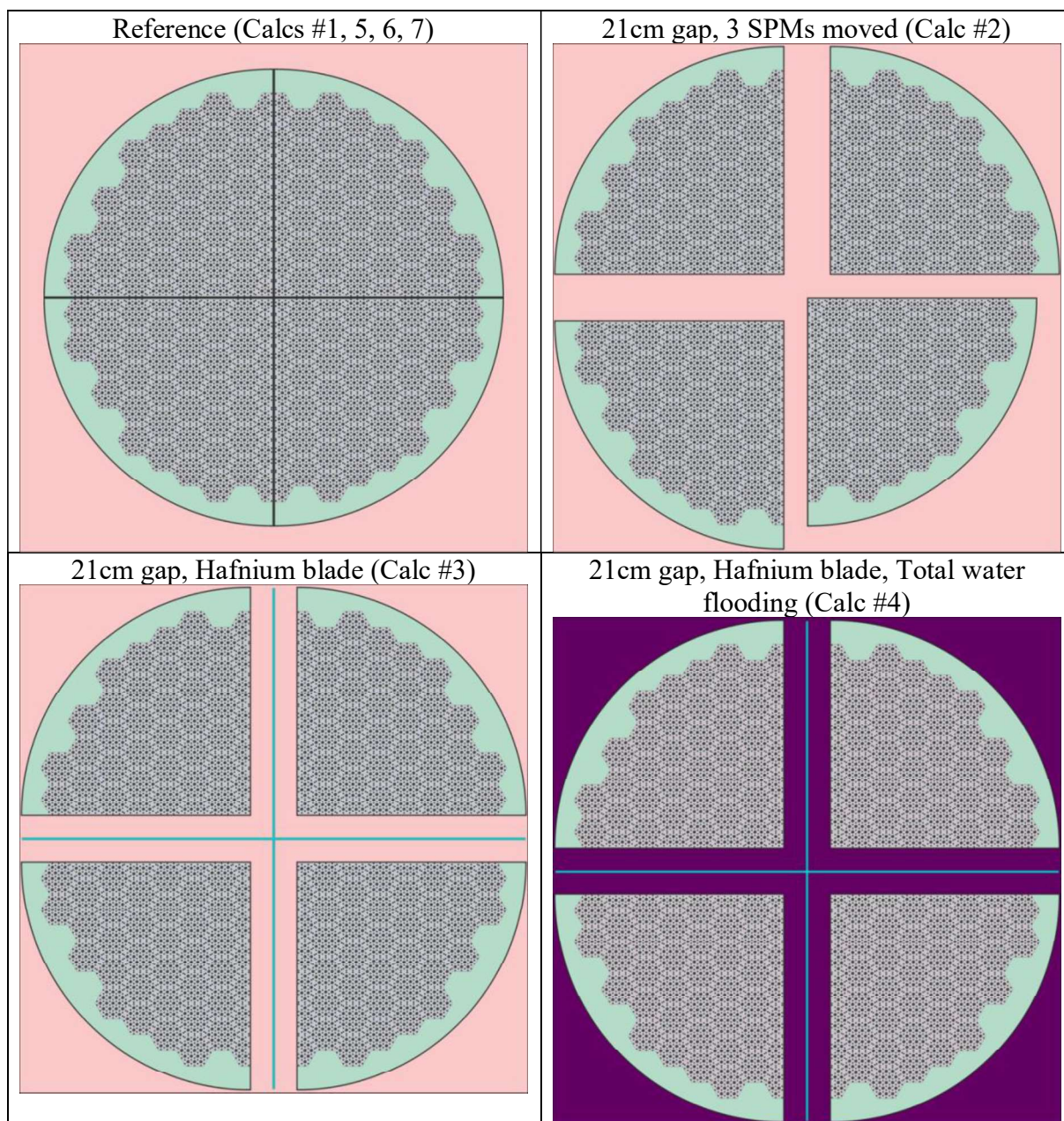
4.2 Results Obtained

4.2.1   Results of the Infinite Cell Benchmark

The results obtained for the infinite cell lattice problem are summarized in Table 4-4. The agreement obtained between OpenMC and SERPENT is very good for calculations #1, 4, 6, and 8. Larger discrepancy up to 140 pcm is observed on calculations #2, #5 and #7, which appears to come from inconsistencies in the thermal scattering library used. The discrepancies in the estimated MDC and FTC coefficients are within the statistical uncertainty of these evaluations. The OpenMC caluation #4 shows that the Doppler Broadening rejection correction for U-238 is

responsible for ~70 pcm. Larger but still reasonable agreement is obtained with the PROTEUS code on the k-eff evaluations. Further investigation is needed for the cases of reactivity calculations.

Table 4-4. Benchmark results comparison for infinite cell problem.

Calc #	XS temp. \ Code	SERPENT	OpenMC (*Δk)	PROTEUS (*Δk)
1	Calculations with all cross-sections at 800K, except for fuel (UCO) at 900K	1.25442 ± 0.00021	1.25444 ± 0.00046 (2)	1.25389 (-53)
2	Calculations with all cross-sections at 300K	1.30220 ± 0.00021	1.30083 ± 0.00042 (-137)	1.30104 (-116)
3	4- with Doppler broadening rejection correction for U-238		1.25821 ± 0.00044	
4	Calculations with all cross-sections at 800K	1.25976 ± 0.00021	1.25974 ± 0.00042 (-2)	1.25687 (-289)
5	#1 - no thermal scattering for Graphite.	1.25516 ± 0.00021	1.25625 ± 0.00043 (109)	1.25328 (-188)
6	#1 - B-10 concentration in Graphite matrix set to 0	1.53602 ± 0.00019	1.53590 ± 0.00038 (-12)	1.53424 (-178)
7	#2 - He coolant in graphite hole replaced with Water	1.38246 ± 0.00017	1.38124 ± 0.00041 (-122)	1.38469 (223)
8	#1 wih Graphite density reduced by 1%	1.25423 ± 0.00021	1.25442 ± 0.00045 (19)	1.25450 (27)
	MDC[pcm/1%] = 1e5*(1/#1 - 1/#8)	-12 ± 30	-1 ± 64 (11)	39 (51)
	FTC[pcm/-100K] = -1e5*(1/#1 - 1/#4)	-338 ± 30	-335 ± 62 (3)	-189 (149)

* Δk : eigenvalue difference from SERPENT, pcm

The k-eff evolutions obtained from OpenMC and SERPENT are compared in Figure 4-6 and show agreement with in ~300 pcm of each other throughout the depletion. Several steps were taken to ensure that SERPENT and OpenMC were using equivalent input parameters for the burnup calculations. Depletion chains which included all relevant nuclei were applied in both codes. In OpenMC, adjustments were made to the standard depletion chain, verified in CASL calculations [10], to include the metastable states of key isotopes, such as Am241, Ag109, etc., to match those included in the SERPENT calculation. Additionally, the recoverable heat values for fission reactions were also adjusted in OpenMC to match those in SERPENT where the recoverable heat from U235 (H_{U235}) is set to 202.27 MeV by default and all other heating values follow the equation:

$$H_i = \frac{Q_i}{Q_{U235}} \cdot H_{U235} \qquad (5)$$

where Q_{U235} is the fission Q-value for U235 (193.72 MeV in SERPENT), Q_i is the Q-value for the isotope of interest, and Hi is the resulting recoverable heat value for the isotope of interest. This formula was used to calculate all heating values in OpenMC based on the ENDF/B-VII.1 data used in both codes.
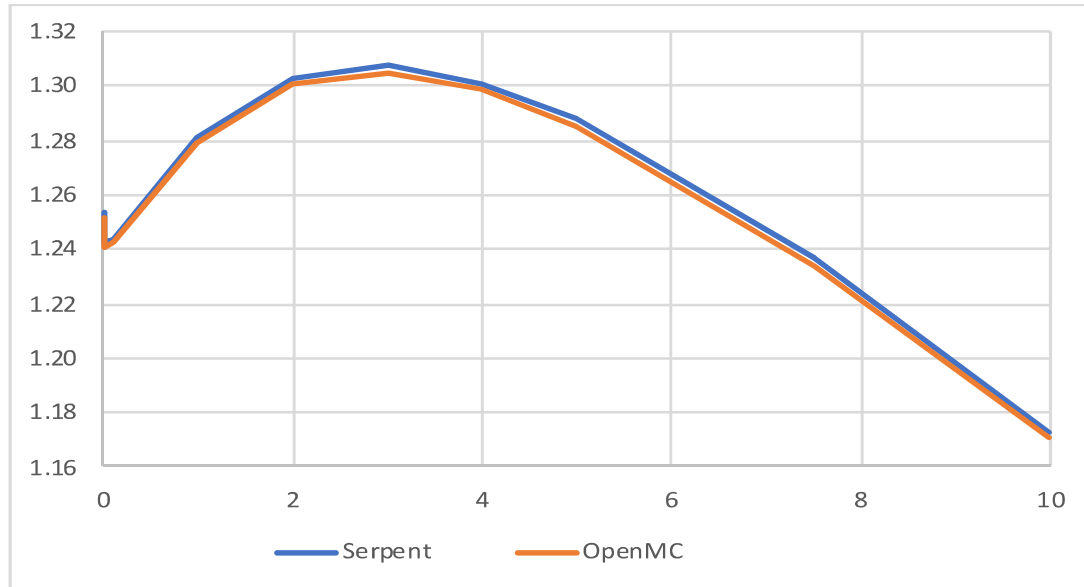
Figure 4-6. K-eff comparison through infinite cell depletion.

4.2.2 Results of the Full Core Benchmark

The results obtained for the full core benchmark problem are summarized in Table 4-5. The agreement obtained between OpenMC and SERPENT is relatively good within 300 pcm of discrepancy. The PROTEUS simulation displays relatively good agreement with ~400 pcm under-estimation on the k-eff, but with consistent results for the MDC and FTC calculations. The k-eff evolution obtained from OpenMC and SERPENT is shown in Figure 4-7 and displays relatively good agreement, with discrepancy consistently less than 300 pcm before 5 EFPY. The isotope densities at the end of the depletion simulations are shown in Table 4-6 and display small discrepancy and relatively consistent between the cell and core benchmarks.

Table 4-5. Benchmark results comparison for full core problem.

Calc #	Description	SERPENT	OpenMC (*Δk)	PROTEUS (*Δk)
1	Reference K-eff	1.06165 ± 0.00016	1.06255 ± 0.00021 (+90)	1.05696 (-418)
2	Reactivity worth at hot shutdown of moving 3 SPMs out of 4, with maximum gap thickness of 21cm	0.92772 ± 0.00018	0.92503 ± 0.00021(-269)	0.92232 (-540)
3	Shutdown margins at cold shutdown with maximum gap thickness of 21cm between each of the 4 SPMs, and insertion of Hafnium blade	0.80582 ± 0.00023	0.80543 ± 0.0002 (-39)	0.79993 (-596)
4	Water flooding at cold shutdown (described in #3) with water (1g/cm^3, 300K) in coolant holes and outside SPMs.	1.04607 ± 0.00018	1.04603 ± 0.00022 (-4)	1.03780 (-827)
5	Moderator density coefficient with reduced graphite density of the fuel pin matrix and the graphite block by 1%	1.05974 ± 0.00016	1.06114 ± 0.0002 (+140)	1.05521 (-453)
6	Doppler coefficient calculated by increasing the temperature of the UCO fuel by 300K	1.05083 ± 0.00015	1.05155 ± 0.00019(+72)	1.04714 (-369)
	MDC[pcm/1%] = 1e5*(1/#1 - 1/#5)	-170 ± 22	-125 ± 30	-157
	FTC[pcm/+300K] = 1e5*(1/#1 - 1/#6)	-970 ± 23	-984 ± 30	-888

* Δk : eigenvalue difference from SERPENT, pcm
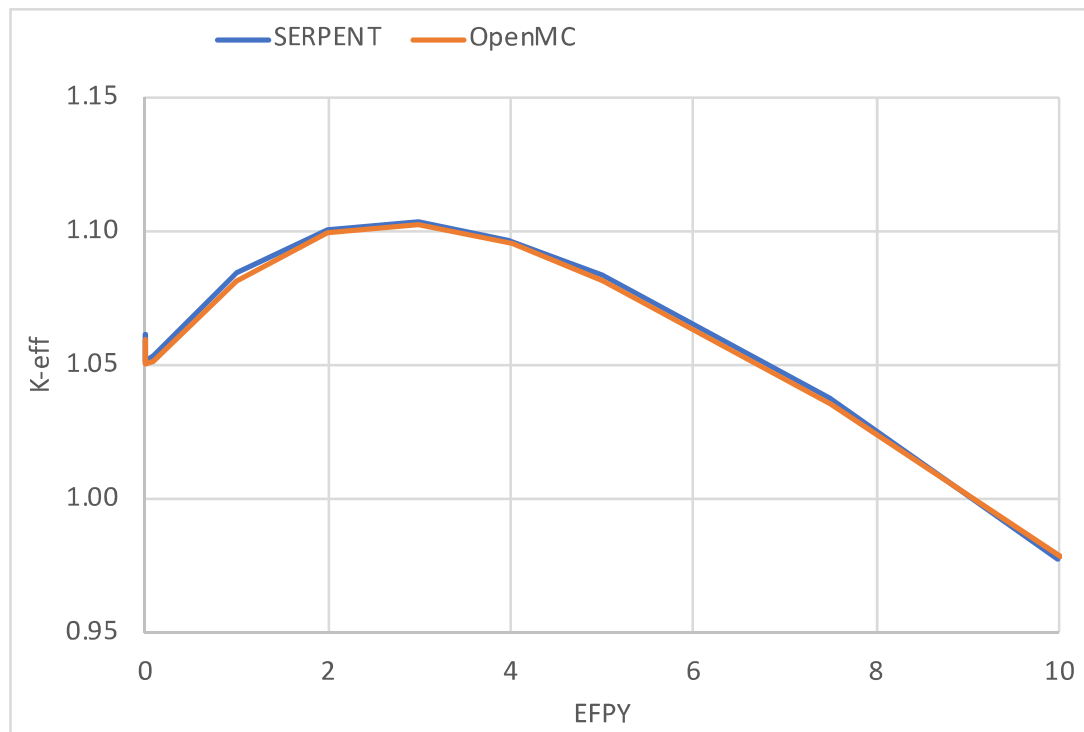
Figure 4-7. K-eff comparison through full-core depletion.

Table 4-6. Weight density comparison for core and cell benchmarks between SERPENT and OpenMC for main depleted isotopes in fuel and graphite matrix regions at the end of depletion.

(SERPENT-OpenMC) SERPENT	Core	Cell
U235	0.1%	-0.2%
U238	0.0%	0.0%
Pu239	-1.1%	-1.1%
Pu240	-1.4%	-1.4%
Pu241	-0.3%	-0.3%
Pu242	-0.5%	-0.3%
Am241	-0.2%	-0.3%
Sr90	0.0%	0.1%
Cs137	-0.2%	-0.1%
Xe135	-2.5%	-2.5%
Sm149	0.4%	0.3%
B10	-0.8%	-0.8%
B11	0.0%	0.0%

5   Additional Detailed Analyses on Optimum Core Configuration

Detailed neutronic and thermal-hydraulics analyses are performed in this section on the optimum core selected in Section 3 in order to provide more details on the power and temperature distributions, to assess the impact from modeling assumptions, and to evaluate alternative design options.

5.1 Detailed Power and Flux from PROTEUS

PROTEUS calculations were performed for 2D and 3D configurations of the Holos benchmark cores. All six core conditions discussed in the previous sections were modeled and simulated using PROTEUS. Since the neutron flux spectra of the six core benchmark cores are very different among calculations 1, 2, 5 and 6, calculation 4, and calculation 5, as can be seen in Figure 5-1, the cross sections were generated from SERPENT calculations of each core with given temperature and material conditions. For core calculations later on, a group optimization study will be performed to determine the number of groups and group structure best fit to the cores of interest.
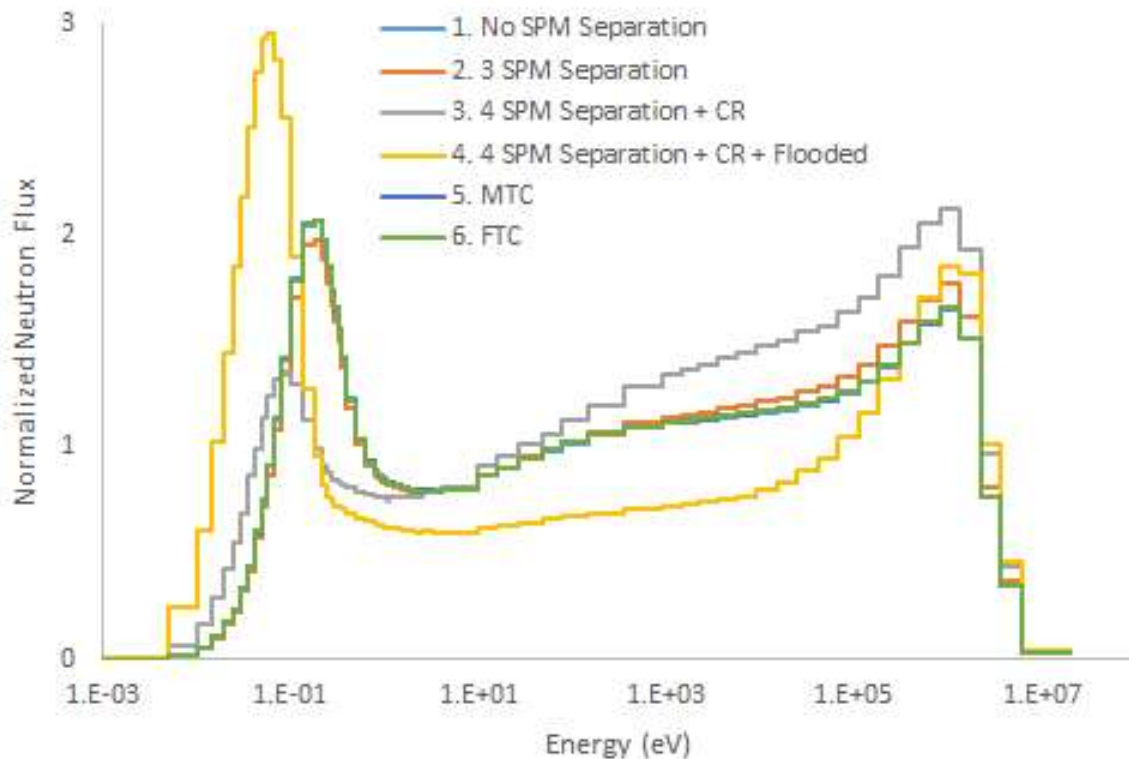
Figure 5-1. Normalized neutron flux spectra of 3D Holos core configurations.

Fast
(0.9 keV –
0.5 MeV)
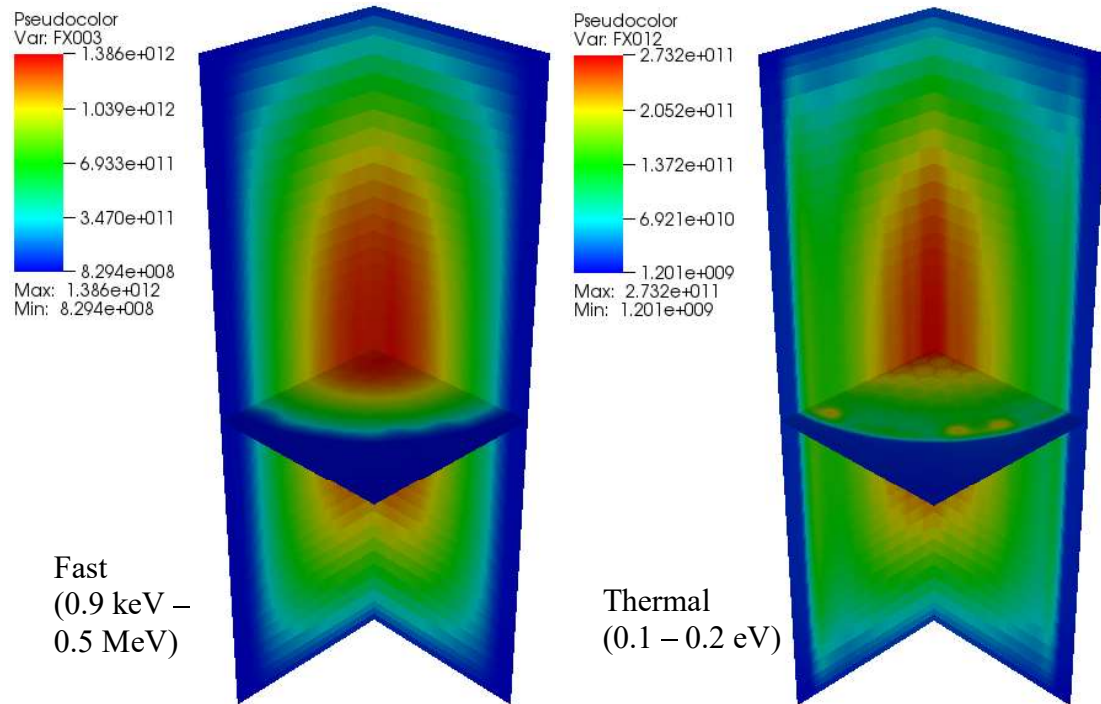
Thermal
(0.1 – 0.2 eV)

Figure 5-2. Neutron flux distributions for calculation 1 (no gap).

3D

2D
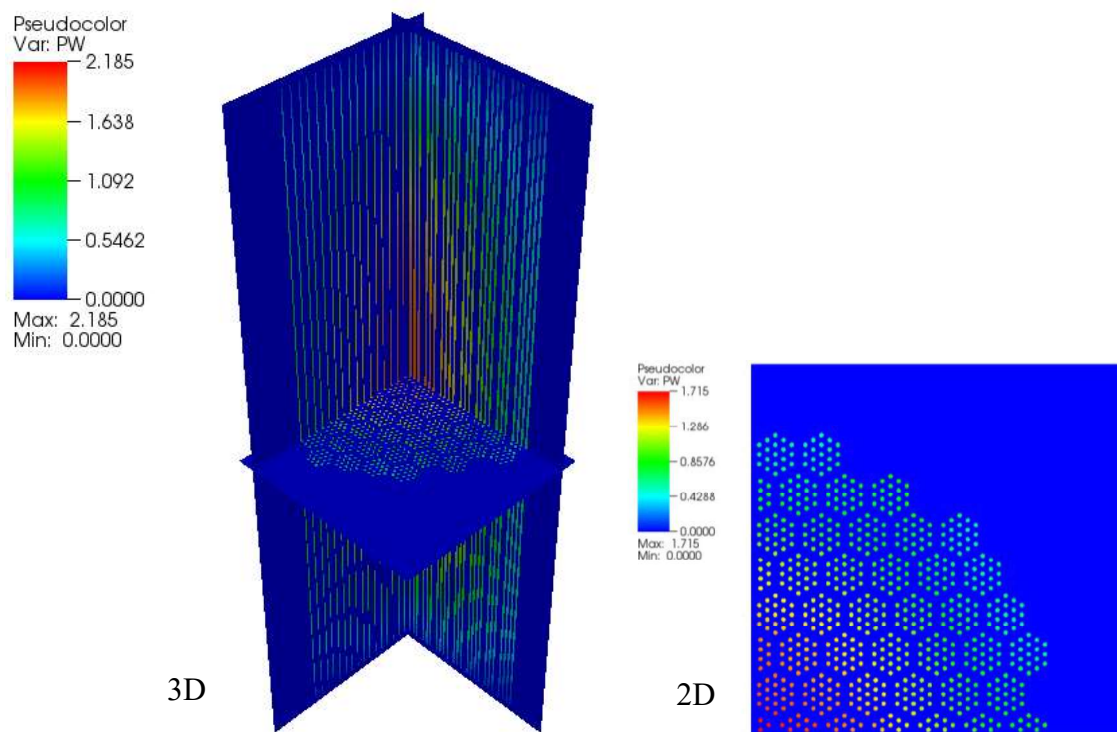
Figure 5-3. 2D and 3D power distributions for calculation 1 (no gap).

Fast
(0.9 keV –
0.5 MeV)
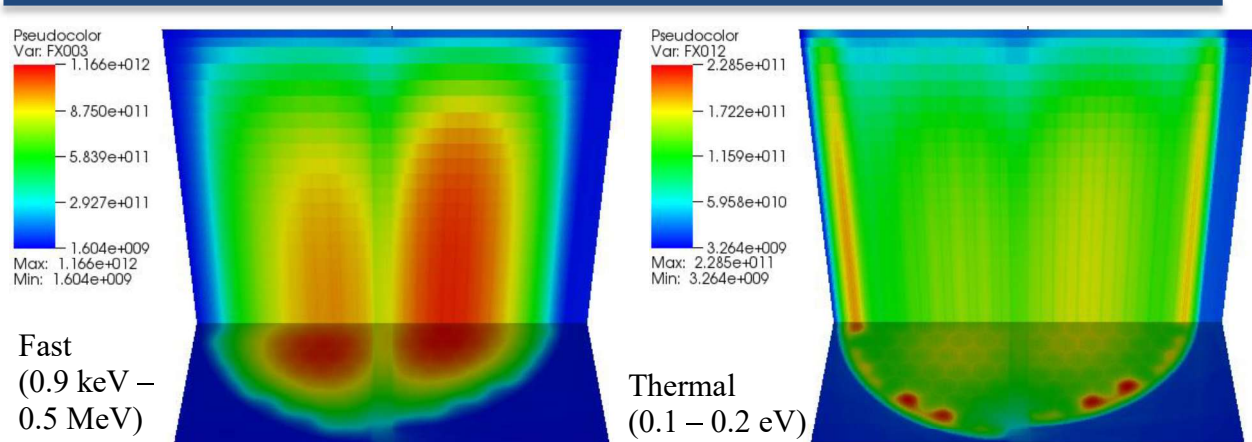
Thermal
(0.1 – 0.2 eV)

Figure 5-4. 3D thermal and fast flux distributions of calculation 2 (3 SPMs separation).

3D

2D
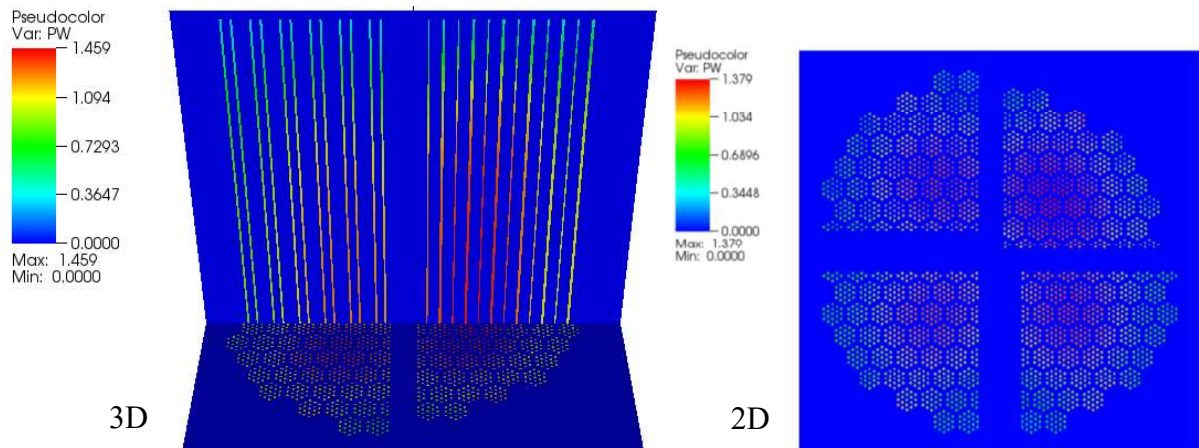
Figure 5-5. 2D and 3D power distributions of calculation 2 (3 SPMs separation).

Since all calculations except calculation 2 are quarter-core symmetric, quarter cores were modeled and calculated. Additionally, since the core is axially half-symmetric (the active core with 390 cm high and the top and bottom reflectors with 5 cm thick), half cores were modeled and calculated for calculation 2. For the verification purpose, unit cells and 2D cores were calculated using PROTEUS and compared with SERPENT solutions. The results of the unit cell calculations are presented in the Section 4.2.1 and the details of the 2D solutions are discussed in Appendix B.

For the selected calculations (calculations 1 and 2), the 3D power and flux distributions produced from PROTEUS are shown in Figure 5-2, Figure 5-3, Figure 5-4, and Figure 5-5. The solutions indicate that the maximum group fluxes of calculations 1 and 2 are 1.37×10^{12} and 1.17×10^{12} #/cm^2·s, respectively, and the maximum relative powers are 2.19 and 1.46. The maximum relative powers for the integrated 2D are approximately 1.72 and 1.38, respectively. Therefore, the axial peak factors for calculations 1 and 2 would be roughly 1.27 and 1.15, respectively.

5.2 Thermal Hydraulic Estimates on Hot and Average Channels

Thermal hydraulic estimates on hot and average channels were performed with SAM to assess the peak and average coolant, structures and fuel temperatures in the core for detailed neutronic analyses. For both average and peak channels, the axial power distribution considered is shown in Figure 5-6, and the radial power peaking (for hot channel) is 1.5868. Those values were provided by PROTEUS on an "earlier core" configuration. The main input parameters are shown in Table 5-1.
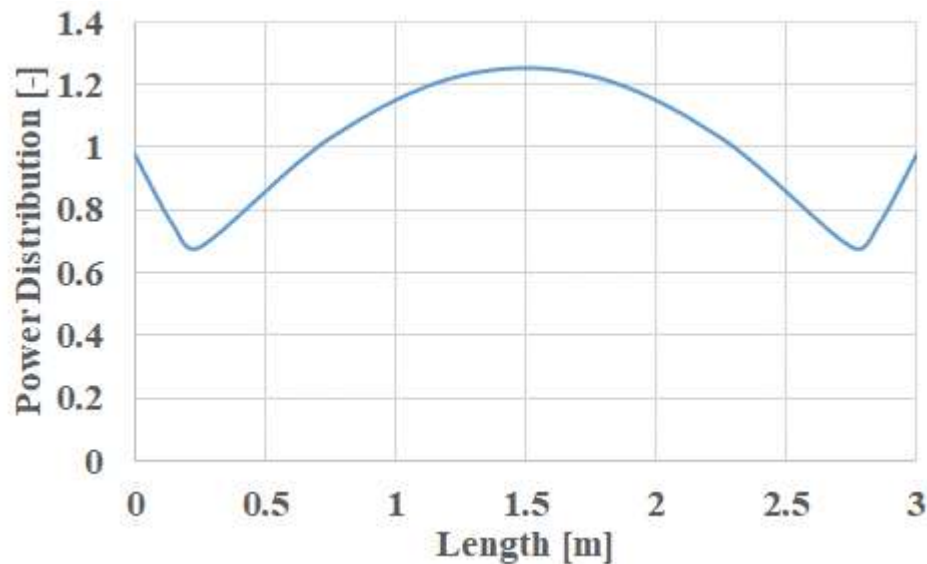
Figure 5-6. Power distribution in active reactor core.

Table 5-1. Operating conditions and SAM Input parameters.

Parameters	Values
Pressure [MPa]	7
mass flow rate per channel [kg/s]	0.00279
Inlet temperature [K]	732.2
Helium density [kg/m^3]	4.55
Channel inner dia. [m]	0.00482
Reynolds	19881.66
Prandtl	0.655644
Cp [j/kg-K]	5188.6
k [W/m-K]	0.2936
Viscosity [Pa.s]	3.71e-5
Friction factor	0.026631
Power per fuel assembly [kW]	Avg = 146 Peak = 231
Surface area density per fuel [1/m]	1696

The SAM core channel model was simulated using the steady solver to directly solve the thermal equilibrium during normal operating conditions. Some of the key results are summarized in Table 5-2. The pressure drop and maximum temperatures for both coolant and fuel were all far from the respective safety limit. The results provided by SAM on the coolant outlet temperatures were verified using an analytical solution.

Table 5-2. SAM calculated maximum values.

	Average channel	Hot channel
Pressure drop (Pa | bar)	63,637 | 0.636	68,473 | 0.685
Max. coolant temp [°C | K]	646 | 919	755 | 1028
Max. fuel temp [°C | K]	719 | 992	878 | 1151
Max. coolant velocity [m/s]	42	47

The temperature distributions along the axial direction are shown in Figure 5-7. The axial distributions of coolant and fuel temperatures are consistent with the power distribution. The calculated external surface temperatures are similar for cladding, lead-buffer and graphite, indicating very small radial temperature gradients across these materials. The temperature distribution across the thickness of heat structure observed significant slope in the fuel region due to low thermal conductivity compared to other heat structures (cladding, lead-buffer and graphite).

Figure 5-7. Temperatures in average and hot coolant channels along the axial direction (solid temperatures are at external surface of each material).

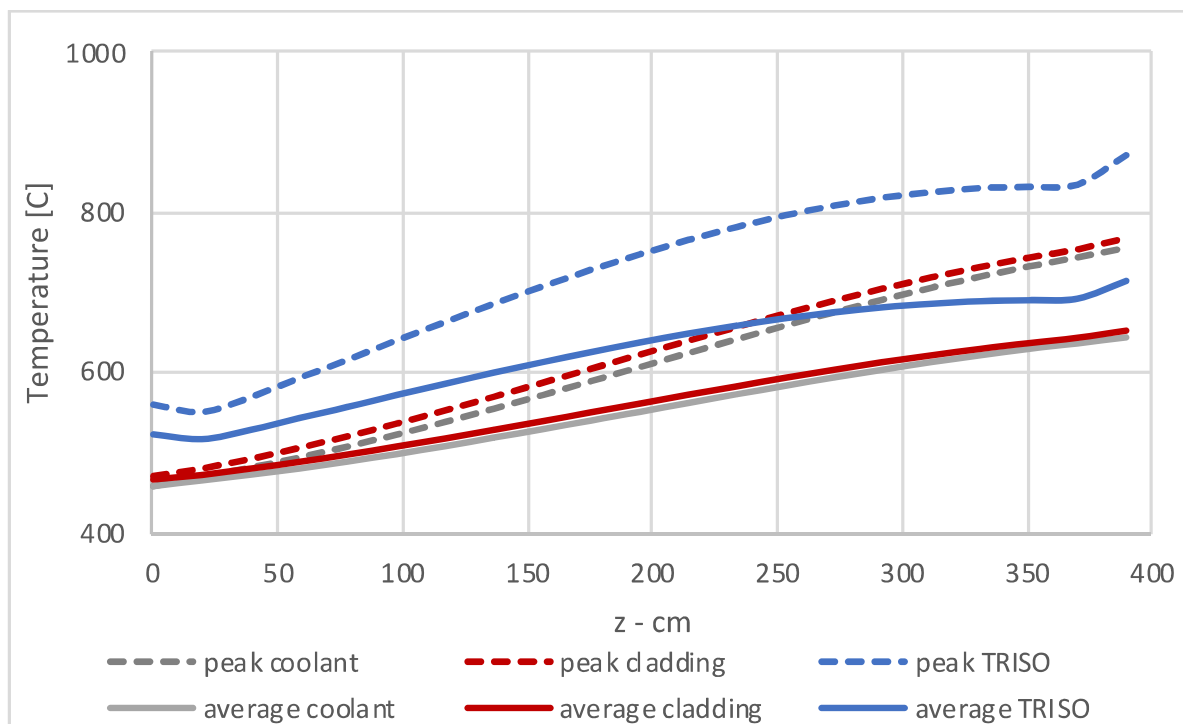The preliminary thermal analysis of the reference HolosGen fuel assembly design was completed using the SAM code. Reasonable simulation results were obtained and verified with analytical solutions. A homogenized pin-cell approach was used in this study for the thermal analysis of the prismatic block type fuel assembly design. To examine the accuracy of this approach, a more detailed model with full 3D representation of the solid structures (heat conduction) and 1D representations of coolant channels (fluid flow) will be pursued.

5.3 Detailed Depletion Analysis

The depletion model used for design optimization work performed in Section 3 considers only one depletion region, meaning that all the fuel and burnable poisons are depleted at the same rate throughout the core (in central region and in more remote regions). The impact from this approximation is assessed in this section, together with the shift in power throughout the depletion. It should be mentioned that for simplification purposes, the depletion calculation performed does not consider any gap in between the four SPMs, while it is expected that varying gap thickness will be used to compensate for the excess reactivity throughout the irradiation.

Detailed depletion calculations were performed on 3 radial zones and 6 axial zones to assess the impact on the core life-time of a refined depletion model, as shown in Figure 5-8. The number of fuel assemblies in each radial region is displayed in Table 5-3 together with the average power per assembly. As expected, the average assembly power in inner assemblies is almost twice as large as that of the outer assemblies. For each of the 18 depletion regions, the averaged fuel and structure temperatures were computed using SAM simulations on three representative assemblies of each channel, as shown in Figure 5-9. Once again, in this study, only the temperatures are varied, not the densities, which would require to account for thermal expansion. This simplification is acceptable for preliminary analysis because the temperature reactivity effect is found to be much more important than the moderator reactivity effect (as shown later in Table 5-6). In these figures, RAD1, RAD2, and RAD3 represent the inner, central, and outer assemblies, while AX1 to AX6 represent the 6 axial regions modeled.
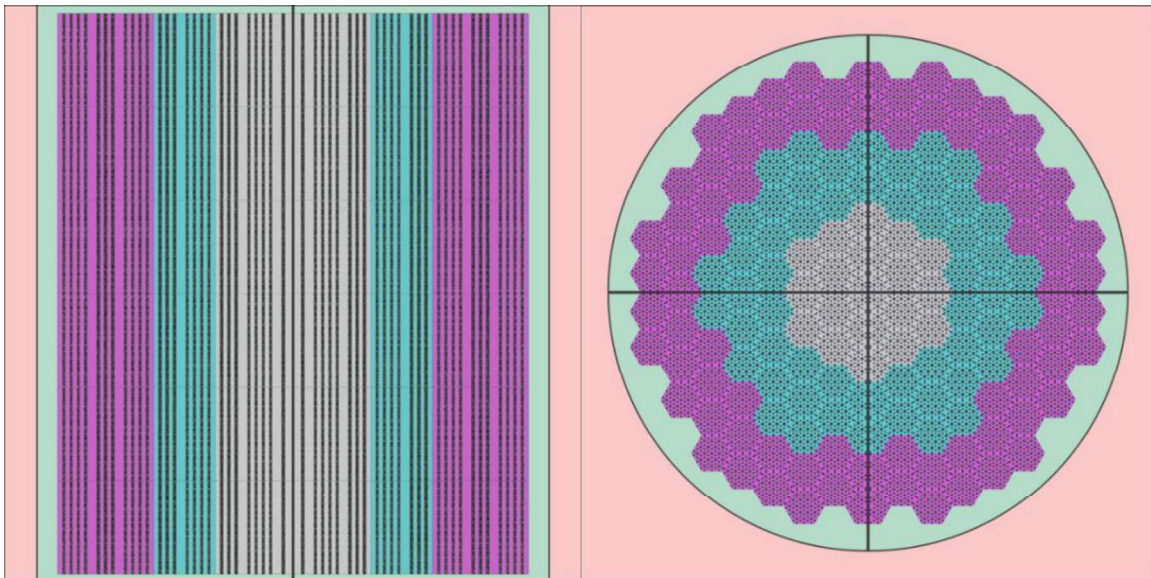
Figure 5-8. Axial and radial layout of the Holos Model with different graphite temperatures in each individual depletion region modeled.

Table 5-3. Description of each radial assembly region.

	Inner	**Middle**	**Outer**
Num. assembly	19	54	78
Avg. power/assembly	0.203MW	0.168MW	0.116MW
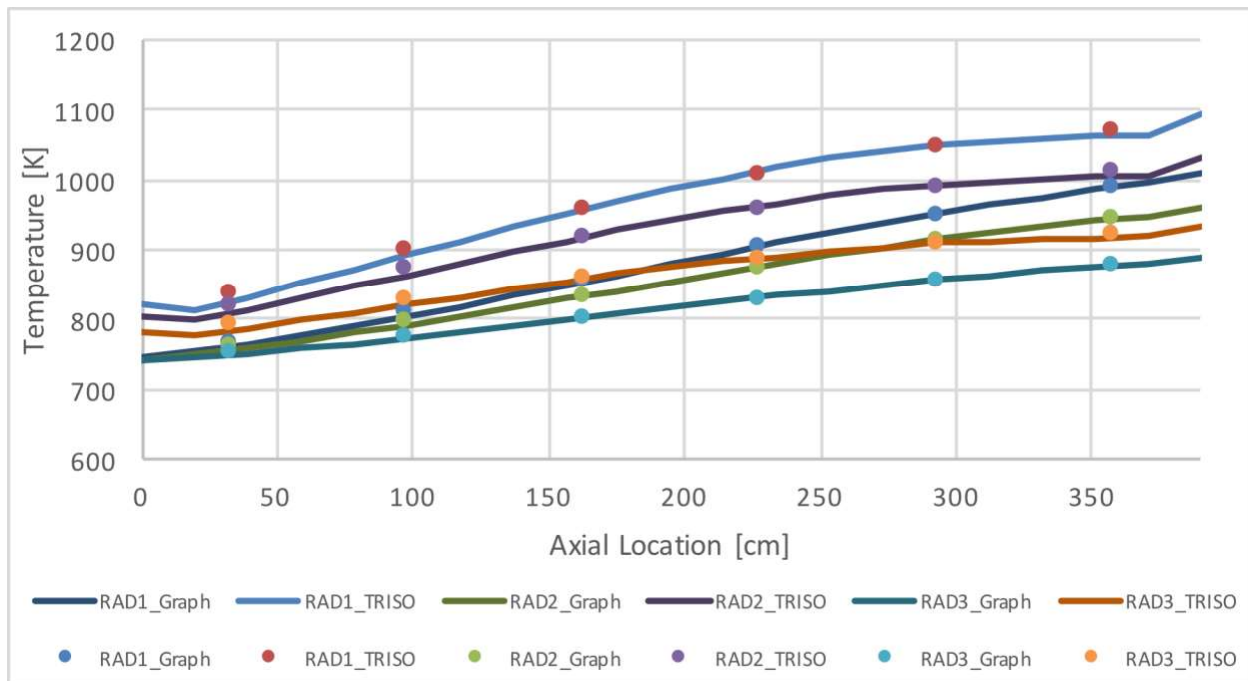
Figure 5-9. Average graphite and fuel temperatures in each region.

Three depletion simulations were performed using SERPENT, and the resulting k-eff evolution through burnup is displayed in Figure 5-10:

- Calculation 1: 1 depletion zone & core averaged temperature

- Calculation 2: 18 depletion zones & core averaged temperature

- Calculation 3: 18 depletion zones & detailed temperature per depletion zone

The impact from using refined zoning for depletion simulation was found to be significant, potentially finding a core lifetime reduced by ~2 years. The refined temperature model, on the other end, does not impact much of the results due to the relatively small variations in fuel and structure temperatures throughout the core. Further increasing the number of depletion zones should be performed in the future in order to verify that the 18 depletion zones selected are sufficient (this was already performed with earlier version of the core model).

The steep reduction in k-eff through burnup in refined depletion model is explained by faster depletion of burnable poisons and of fuel in central core region (RAD1_AX3&4), as shown in Figure 5-11 and Figure 5-12. The simplified depletion model used for core optimization only considers one depletion region, meaning that all the fuel and burnable poisons are depleted at the

same rate throughout the core (in central region and in more remote regions). Even though this overly simplified depletion model provides optimistic results, these are realistic results we should lean toward with proper flattening of the power map obtained with different enrichment zones, packing fraction zones, and concentrations of burnable poisons. Such optimization should be performed in a second step of the design optimization of the Holos-Quad in order to maintain a core life-time of 8 EFPY using detailed depletion model.
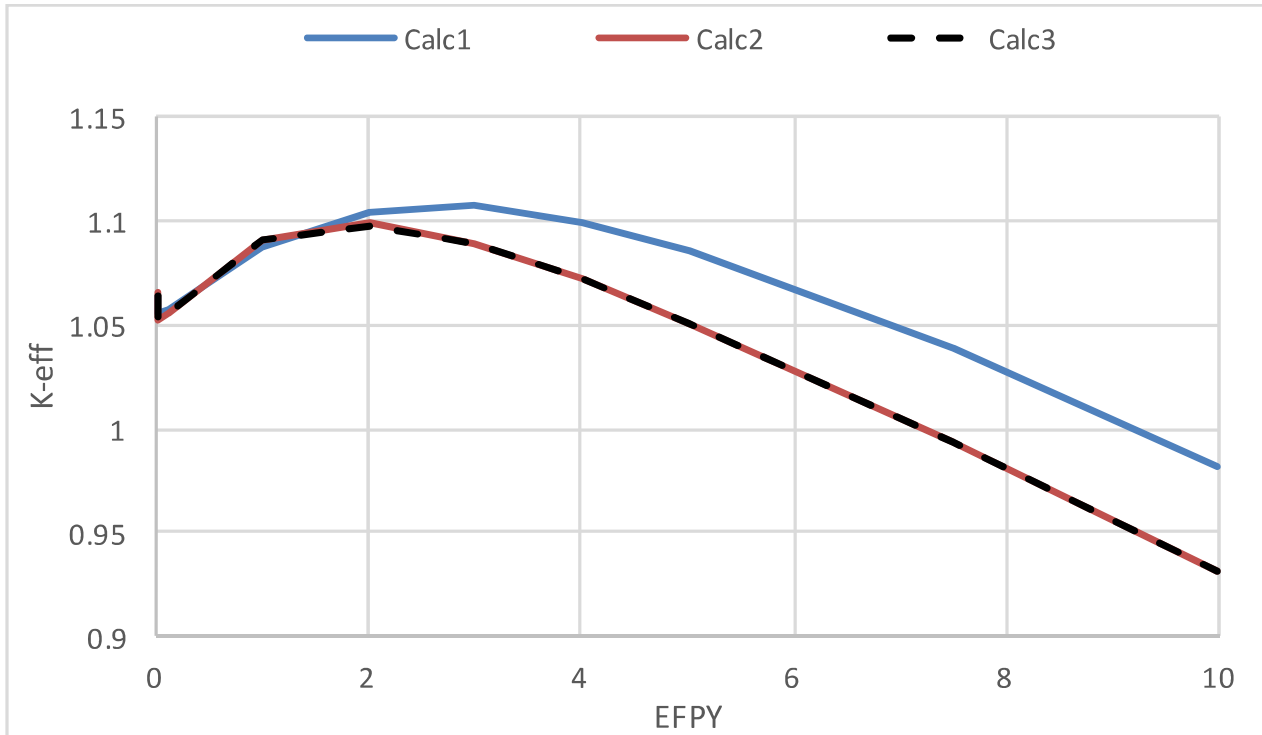
Figure 5-10. K-eff burnup evolution with different depletion zones.
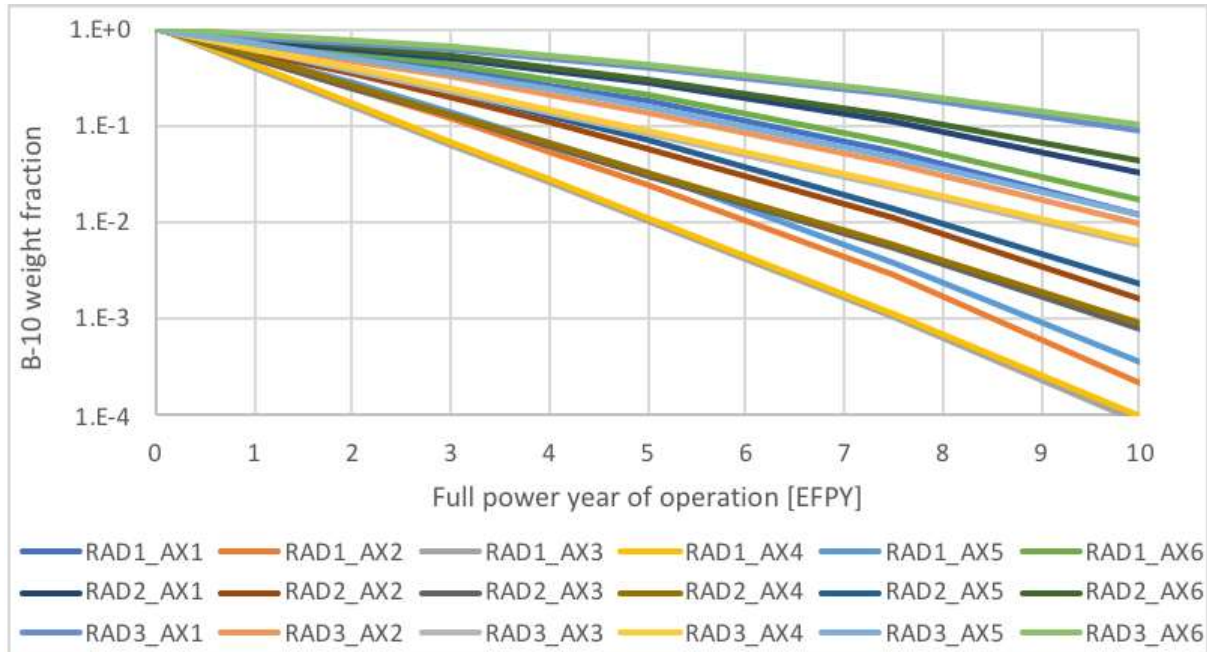
Figure 5-11. Axial and Radial variation of B-10 burnable poison concentration.
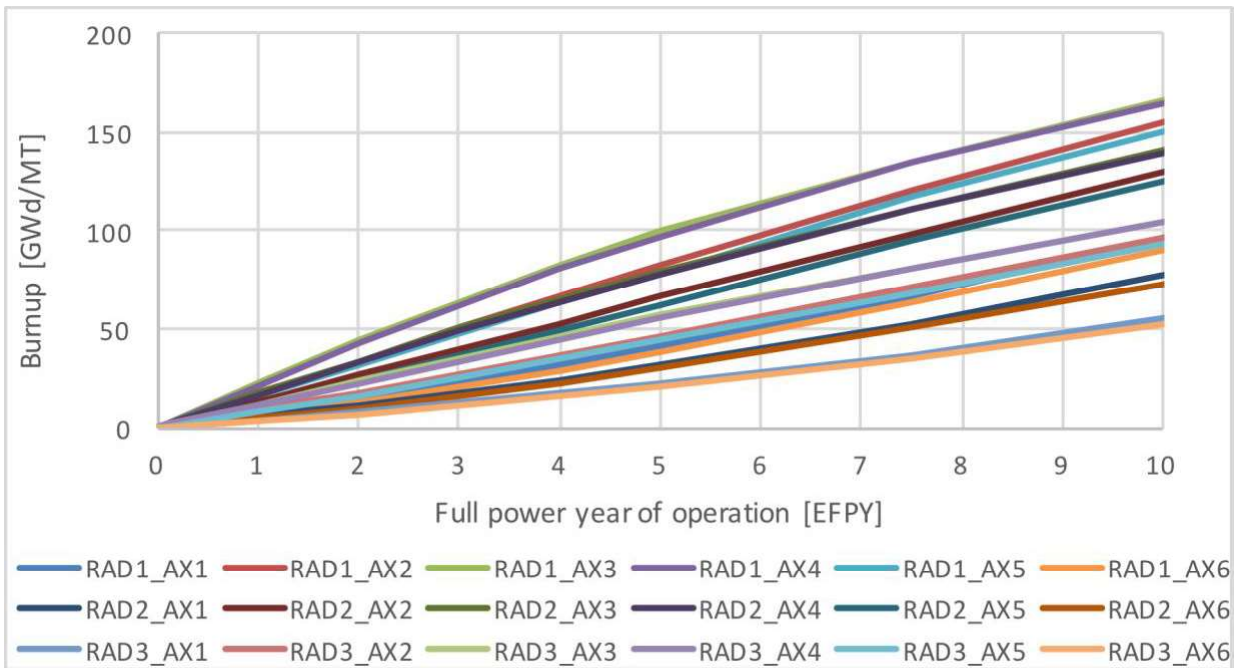
Figure 5-12. Axial and Radial variation of burnup.

Finally, the power shift through depletion was assessed throughout each core regions. As expected, the total power in central assemblies (RAD1) is reduced through depletion, while it increases in the outer assemblies (RAD3), as shown in Figure 5-13. In a similar way, the power in the central axial regions (AX3 and AX4) significantly drops throughout the depletion, while the power in the lower (AX1) and upper regions (AX6) increases, as displayed in Figure 5-14.
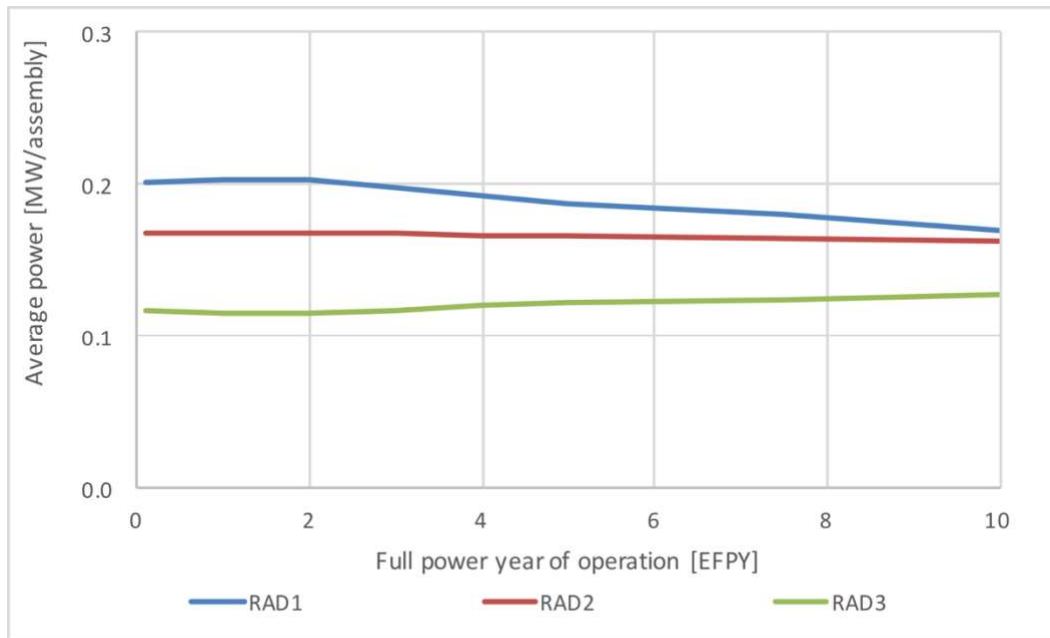
Figure 5-13. Power shift through depletion from inner to outer assembly region.
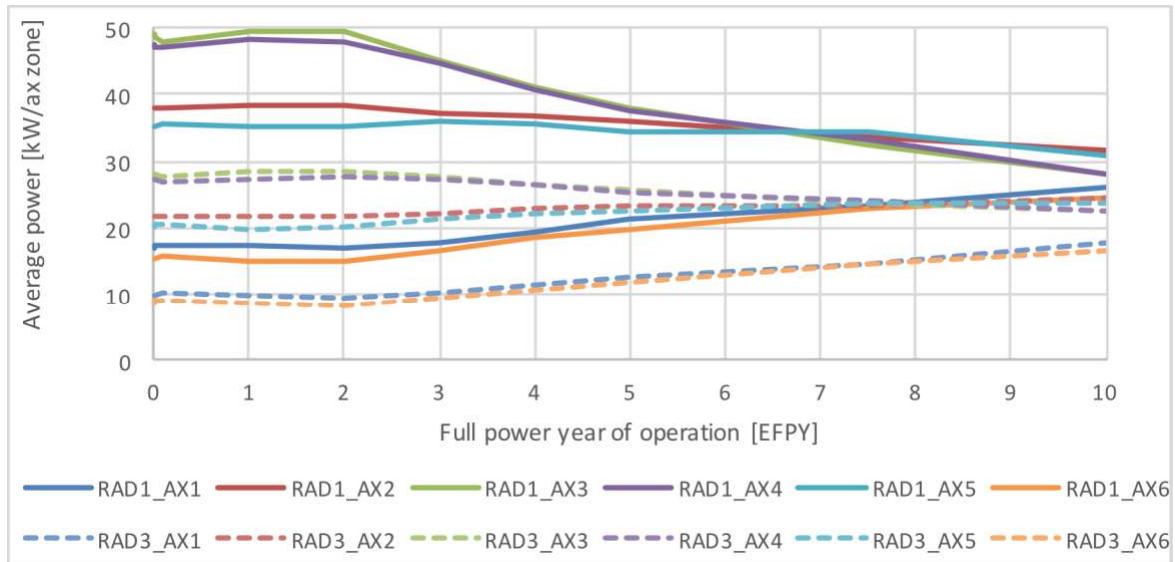
Figure 5-14. Power shift through depletion in different axial regions.

5.4 Assessment of Xenon Reactivity Effect

The xenon poisoning of a nuclear reactor affects its load following capability by providing reduced/increased reactivity after drop or increase in neutron power. In order to assure operational flexibility of the Holos-Quad throughout its lifetime, an excess of reactivity of 2,000 pcm was initially targeted (as explained in Section 3.1.1). This section provides a preliminary estimate of the xenon poisoning effect by assessing the initial reactivity drop due to equilibrium xenon concentration. For this analysis, the single-region depletion model was employed to model 10 EFPDs using SERPENT, as shown in Figure 5-15. The reactivity is found to drop by ~1,000

pcm within ~1.5 days of full power operation as xenon fission product concentration reaches equilibrium. This is much smaller than the 2,000 pcm initially considered suggesting that we were conservative in our approach. However, future analysis should model transient simulations with large variations of power at the end of life to verify the excess of reactivity remains sufficient to compensate for increase in the xenon level.
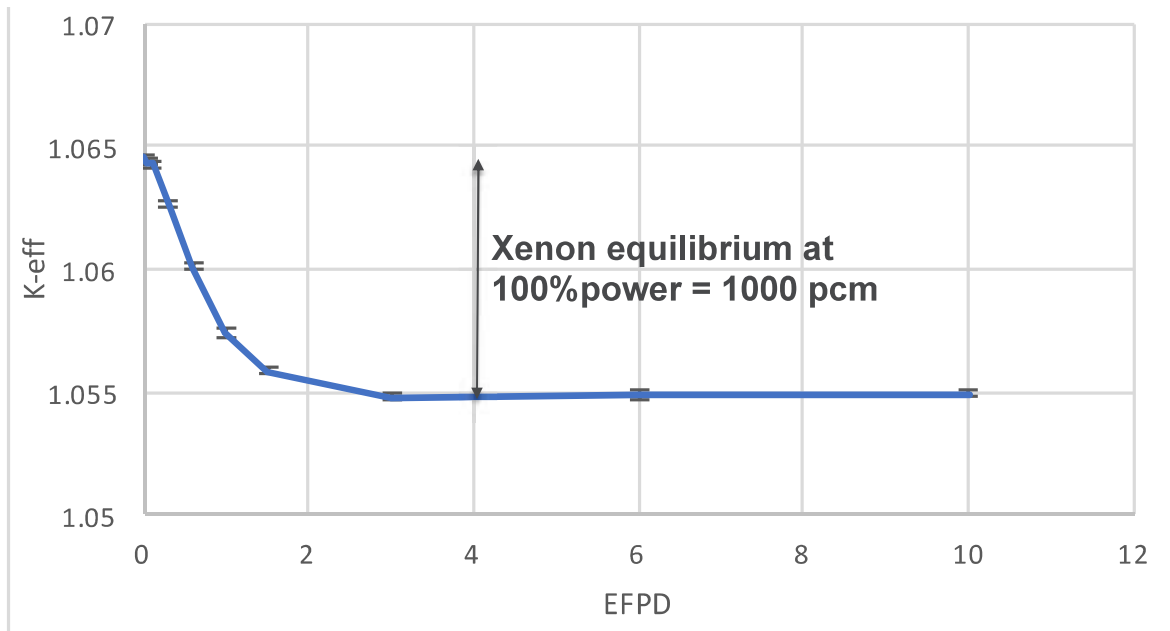
Figure 5-15. K-eff evolution in first 10 days of irradiation.

5.5 Impact from Alternative Reflector Material

Beryllium metal was initially considered as reflector material due to its outstanding reflector performance and relatively small weight density (1.778 g/cm^3). However, its relatively low melting points (~1,290°C) may be an issue during decay heat removal scenarios, and its toxicity makes it unattractive. Alternative reflector materials were investigated to assess the impact of switching to BeO (density ~2.60 g/cm^3 and melting point ~2,500 $^\circ$C) and Graphite (density ~1.80 g/cm^3) in the axial and radial reflectors of the optimized Holos-Quad.

This preliminary analysis only considers the neutronic impact on k-eff at BOL and results are summarized in Table 5-4. The axial reflector type has very small impact on the results. The radial reflector type displays much larger impact. Beryllium metal is found, as expected, to be the best reflector candidate. BeO does provide relatively reduced reflector performance, with about 700 pcm of penalty on k-eff at BOL, but a significant increase in associated core weight by ~2.5 tons (the reflector weight in the optimum configuration represents 5.5 tons out of a total weight of 26.7 tons). Finally, graphite reflector shows a penalty on k-eff at BOL of ~3,000 pcm, but significantly reduced impact on total core weight.
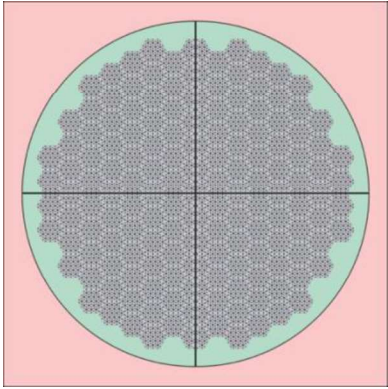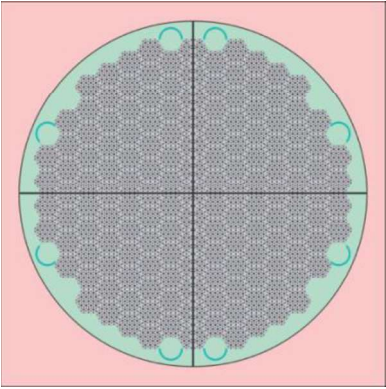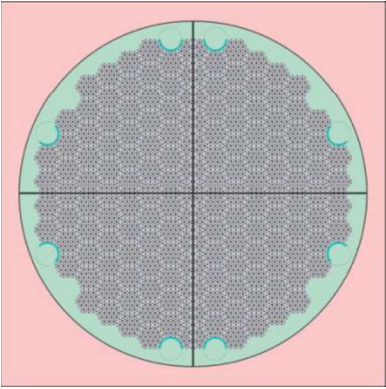
Table 5-4. Impact of reflector type on k-eff.

Axial reflector (~5cm)	Radial reflector (~7cm)	K-eff ± σ	ΔK-eff (vs. 1st line)
Be	**Be**	1.06387 ± 0.00033	**0**
Be	BeO	1.05691 ± 0.00031	-0.007
BeO	Be	1.06413 ± 0.00035	0
BeO	BeO	1.05674 ± 0.00033	-0.007
Graphite	Be	1.06417 ± 0.00031	0
Be	Graphite	1.03611 ± 0.00037	-0.028
Graphite	Graphite	1.03495 ± 0.00036	-0.029

5.6 Initial Investigation of Secondary Control System

The Holos-Quad core consists of four SPMs and adopts a non-traditional primary reactivity control mechanism: the criticality is achieved by moving the two SPMs closer, while the reactor is shut down by moving the modules away. Secondary reactivity control system is being developed within this project to meet redundancy requirements. Two independent reactivity control systems are required as each must be able to provide sufficient negative reactivity worth to bring the reactor from any operating conditions to shutdown condition by assuming that one of the reactive control systems is inoperative at a full power operating condition. A preliminary design of hafnium blades inserted in between the four SPMs were already considered during the optimization process (see Section 3.1) to provide additional shutdown margins during cold shutdown and transportation.

Table 5-5. Preliminary assessment of drums control system.

No Drums	Drums Out	Drums In
K-eff = 1.065	**K-eff(1.0cm) = 1.051**	**K-eff(1.0cm) = 1.029**
	K-eff(0.5cm) = 1.051	**K-eff(0.5cm) = 1.032**

This section provides a very preliminary estimate of a secondary control system based on rotating absorbing drums. Such systems have been developed in the past especially targeting reactors for space application [11]. In this study summarized in Table 5-5, the drums investigated are made of Be, with a thin layer of hafnium material (1.0cm and 0.5cm were investigated) with a 180°C angle. Inserting the drums in the core with all absorbing regions leaning toward the outside, the penalty on k-eff is found to be ~1,400 pcm. This penalty will need to be compensated by additional fuel/moderator or by reduced core lifetime. Fully rotating the eight drums towards the core provides 1,800 to 2,200 pcm of reactivity worth, depending on the thickness of the hafnium blade. Future work will investigate additional drum locations, alternative poison material (B_4C), and optimize the angle of poison layer.

5.7 Preliminary Reactivity Effects Assessment

In order to inform preliminary control system analysis performed by the ARPA-E resource team, a preliminary estimate of the reactivity control systems was performed at BOL, and results are summarized in Table 5-6. Even though the MDC provides negative reactivity feedback, it is very small due to the presence of diluted burnable poisons in the graphite moderator. Consequently, the fuel temperature coefficient is the primary negative neutronic feedback considered in this study. The reactivity worth from different control systems under investigation are displayed in Table 5-6 together with the reactivity effects needed to be compensated for reactor operation. The separation of 4 SPMs with a gap of ~21 cm leads to significant reactivity drop (18,000 pcm), which is more than enough to compensate for the current excess reactivity throughout burnup (almost 10,000 pcm) and the full power to cold shutdown reactivity (~5,000 pcm). If one SPM fails to move, the 3 remaining SPMs provide enough shutdown margin (14,000 pcm) to achieve hot shutdown with >2,000 pcm of reactivity margins, which was one of the optimization constraints implemented in Section 3.1.3. Reducing the excess reactivity will be attempted in the future by employing alternative burnable poisons. This would indeed significantly help reducing the gap required for the SPMs.

Preliminary estimates on the secondary control system discussed in Table 5-5 show that rotating 8 drums located in radial reflector regions provides ~1,800 pcm of reactivity worth, which may already be sufficient to compensate the ~500 pcm required to go from full power operation to hot shutdown, and ~1,000 pcm is required to compensate the xenon reactivity effect. It should be noted that lower temperature assumed for the hot shutdown state will increase reactivity worth requirements.

Future analysis will focus on detailed evaluation of shutdown margins for both primary and secondary control systems and will include uncertainties and reactivity faults.

Table 5-6. Assessment of reactivity controls at BOL.

Moderator density coefficient	pcm/%dens pcm/K	-145 ± 23 -0.3 ± 0.05
Fuel temperature coefficient	pcm/K	-3.2 ± 0.07
SMP separation	pcm/cm - 1SPM sep. pcm - 4SPM max sep. pcm – 3SPM max sep.	-235 ± 28 $-18,105 \pm 42$ $-13,966 \pm 42$
Hf blade	pcm	$-17,820 \pm 51$
Control drum rotation (all)	pcm	$-1,814 \pm 69$
Xenon reactivity effect	pcm	~1,000
Max. excess reactivity	pcm	$+9,677 \pm 35$
Full power to hot shutdown	pcm	$+443 \pm 41$
Hot shutdown to cold shutdown	pcm	$+4,280 \pm 41$

6   Preliminary Shielding Analysis

Shielding analysis is being performed for the Holos reactor concept by the ARPA-E resource team, and preliminary results are summarized in this report. The shielding requirement was assessed for the equipment or components in the ISO container near the core in Section 6.2. The focus is on the turbomachinery since it is located closer to the core. Another shielding analysis presented in Section 6.3 focused on assessing the thickness of the building wall outside the ISO container to meet personnel dose rate limits outside the reactor building. Finally, the shielding requirements during transportation of a used SPM in an ISO container was evaluated in Section 6.4. Throughout this shielding study, the preliminary core model investigated prior to the core optimization performed in this report was used. Even though the core design changed quite significantly (increased in driver fuel length, from 3.0m to 3.9m, reduction in number of assemblies from 235 to 151, increase in pin pitch, etc.), the main conclusions from the shielding analysis proposed here will remain applicable to the optimized Holos-Quad, but future work will focus on updating this study.

6.1 Methods Description for Shielding Analyses

For these preliminary analyses, the MCNP6.2 [12] code was employed for the particle transport calculation. The weight window variance reduction technique was employed. This is required to obtain results with sufficiently small statistical uncertainty in a reasonable amount of time. The weight window was generated by the ADVANTG [13] code for each case investigated. The major radiation source responsible for the irradiation damage on the equipment and the personnel working outside the reactor building during operation consists of fission neutrons. This fission neutron sources were generated with an eigenvalue MCNP6.2 calculation. All subsequent evaluations relied on this criticality source for shielding analysis.

6.2 Shielding Requirements on the Turbine

A quarter of the core was modeled with reflective boundary condition on the left and bottom boundary. A 10cm gap in between SPMs was included in the model for conservatism. Thus, neutrons can stream through the center gap during operation when the submodules are separated apart from each other. Due to this neutron streaming, both the axial and side shield may be needed to protect the turbine as illustrated in Figure 6-1 and Figure 6-2. Based on this shielding configuration, several cases were investigated with different shield thickness. The shield is assumed to be composed of 50% B_4C and 20% SS316. Irradiation damage on the equipment is calculated considering a thermal power of 5.5 MWt for one SPM in the model over a lifetime of 8 EFPY.

The results for all the cases investigated are summarized in Table 6-1. The results show that it is important to include the side shield to prevent the streaming neutrons from reaching the turbine. This is also illustrated in Figure 6-3, which shows that the side shield effectively blocks the neutron from reaching the turbine region. To determine the thickness of the shield required, it is necessary to have a DPA limit on the turbine. We cannot rely on the background neutron flux level limitation because that would require shield thickness larger than 2m. Thus, additional information on the DPA limit on the turbine blades is required. In particular, experiments would be needed to understand the detailed failure mechanism of turbine due to radiation damage and the DPA limit associated with it. For this study, we assume that the material swelling rate would be the limiting factor for the turbine, which is negligible below 1 DPA. If this is the DPA limit,

then no shield is needed for protecting the turbine. If 0.1 DPA limit is used, then 5cm axial and side shields would be needed.
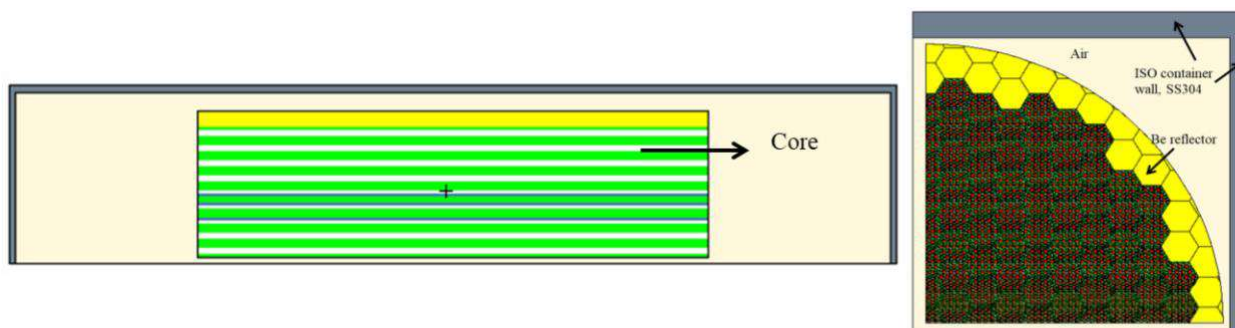
Figure 6-1. Axial (left) and radial (right) core model employed for the turbine DPA.
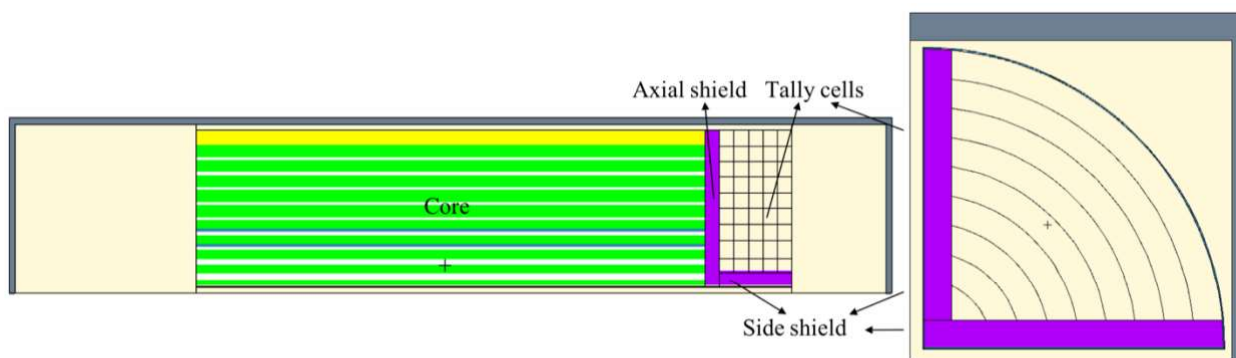
Figure 6-2. Shield configuration for the MCNP model of the Holos reactor concept.

Table 6-1. DPA as a function of shield thickness.

Axial shield (cm)	Side shield (cm)	DPA	Relative STD
0	0	0.15	0.77%
0	5	0.13	0.42%
5	0	0.11	0.90%
5	5	0.09	1.18%
10	10	0.04	0.31%
15	15	0.02	0.26%
20	20	0.01	0.65%
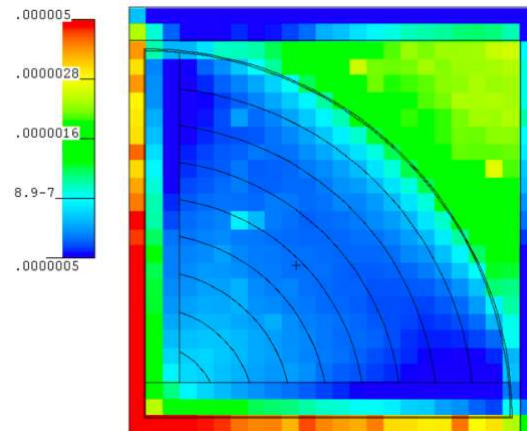
Figure 6-3. Radial neutron flux distribution (#/cm^2/source particle) at the axial location just outside the core.

6.3 Shielding Requirements of the Reactor Building

The ISO container that contains the Holos reactor core will be located inside a reactor building. The dose rate limit outside the building wall is currently assumed to be 10 mrem/hr during operation (at 100% nominal power). Shielding analysis was performed for the building wall of different thickness and material. A typical MCNP model is shown in Figure 6-4. The neutron dose rate just outside the external surface of the building wall for all the cases are listed in Table 6-2. Steel (SS304) is less effective at shielding when compared to concrete due to its worse neutron moderation ability. A mixture of concrete and steel is the most effective building wall material to reduce neutron flux. The optimal volume fractions of concrete and steel can be searched for real design. However, for this preliminary study, the mixture was assumed to be homogeneous with 50% concrete and 50% steel in volume fraction.
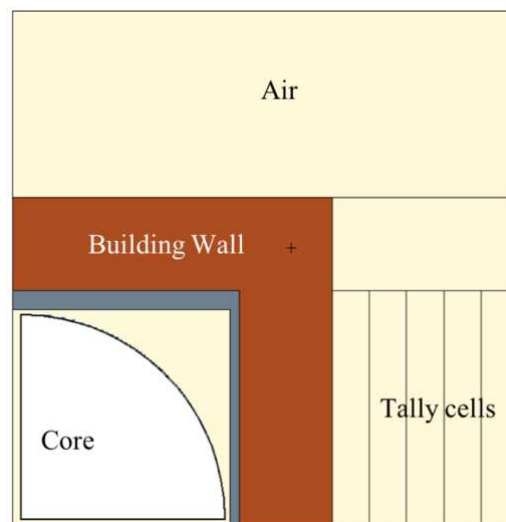
Figure 6-4. MCNP model for dose rate evaluation.

Table 6-2. Neutron dose rate outside the building.

Building Wall		Dose rate (mrem/hr)	Relative STD
Material	Thickness (cm)		
Concrete	50	8.06E+07	2.11%
Concrete	100	4.57E+05	0.57%
Concrete	150	4.10E+03	0.90%
Concrete	200	4.07E+01	1.38%
Concrete	250	4.43E-01	3.27%
Steel	50	1.23E+09	0.25%
50% Concrete + 50% Steel	50	4.09E+07	0.19%
50% Concrete + 50% Steel	100	3.03E+04	0.42%
50% Concrete + 50% Steel	150	2.25E+01	0.41%
50% Concrete + 50% Steel	200	1.75E-02	0.67%
50% Concrete + 50% Steel	160	5.37E+00	0.52%

It requires about 220 cm concrete or 160 cm concrete-steel mixture to reduce the neutron dose rate below 10 mrem/hr. For the case using 160 cm concrete-steel mixture, the prompt photon dose rate is about 3.36 mrem/hr with a relative standard deviation of 0.17%. Nuclear fission also releases delayed photons that carry approximately the same amount of energy as prompt photons (for U-235, the prompt and delayed photon energy are about 6.6 and 6.3 MeV). Thus, for a conservative approximation, the prompt photon dose rate was multiplied by a factor of two to account for the delayed photon contribution. This yields a total dose rate (neutron + photon) of 12.1 mrem/hr, which is only slightly higher than the limit. Consequently, the dose rate limit can be easily satisfied by slightly increasing the wall thickness (~165 cm).

A perimeter at some distance away from the building needs to be set up for the unrestrictive access area. The distance was evaluated assuming the occupational annual dose rate of 5 rem, which translates to 0.57 mrem/hr for 8,760 hr (365 days x 24 hr/day). For a conservative approach, the dose rate is assumed to be inversely proportional to the distance "R" away from the building. This assumes the reactor represents an infinitely long line source. For the practical case, a point source is more representative when R is much greater than the reactor size (~ 2m x 3m), in which case the dose rate would be inversely proportional to R^2. For this preliminary study, the conservative approach was adopted, and R was calculated to be about 20m.

6.4 Shielding Requirements during Transportation

The shielding requirements are assessed for transportation of an irradiated Holos-Quad SPM. According to Ref. [14], the dose rate at the surface of the container is limited to 200 mrem/hr. After reactor shutdown, all the fission neutrons will diminish within seconds, and only the photons from fission products and activation products would contribute to the dose rate. The SCALE [15] code package was employed to perform the depletion calculation of the HolosGen reactor core. A single fuel element was modeled with reflective boundary condition. The fuel was depleted for 3,000 EFPDs, the equivalent of approximately 8 years of operations with a 22MWt coupled core, with a discharge burnup of 64 MWd/kg. The ORIGEN-S module in the SCALE package was employed to evaluate the photon source at different time after shutdown. The photon source at 24, 48, and 72 hours after shutdown is listed in Table 6-3.

Table 6-3. Photon source per 1 MT heavy metal for the discharge fuel of the HolosGen reactor.

Upper E (MeV)	Photon source (photons/s/MTiHM)		
	24h	48h	72h
0.02	2.80E+17	2.13E+17	1.63E+17
0.03	3.93E+16	3.14E+16	2.55E+16
0.05	5.94E+16	4.96E+16	4.26E+16
0.07	2.11E+16	1.70E+16	1.39E+16
0.10	4.85E+16	4.04E+16	3.38E+16
0.15	2.36E+17	1.84E+17	1.45E+17
0.30	1.72E+17	1.20E+17	8.90E+16
0.45	4.70E+16	4.00E+16	3.49E+16
0.70	1.63E+17	1.26E+17	1.08E+17
1.00	1.51E+17	1.31E+17	1.20E+17
1.50	1.80E+16	1.10E+16	8.57E+15
2.00	3.76E+16	3.52E+16	3.37E+16
2.50	1.37E+15	1.13E+15	1.03E+15
3.00	1.37E+15	1.32E+15	1.27E+15
4.00	1.10E+13	1.03E+13	9.86E+12
6.00	1.09E+11	3.38E+08	2.79E+07
8.00	3.12E+06	3.11E+06	3.10E+06
11.00	3.58E+05	3.57E+05	3.56E+05
Total	1.28E+18	1.00E+18	8.19E+17

This photon source was used for transport calculations to evaluate the dose rate on the surface of the container. The transport calculation was performed with MCNP6.2 with weight window generated by ADVANTG. The ISO container transports only a single irradiated SPM. The photon source is assumed to be uniformly distributed radially. This is a conservative approach since this re-distributes the photons that should peak at the fuel center to the core periphery. Thus, in this approach, more photons are likely to get out of the core.

Lead shield was used for photon shielding in this preliminary study. The SPM position within the container is carefully chosen as shown in Figure 6-5, so that dose rate on the left surface of the container would be the highest.

The dose rates on the left outer surface of the container are listed in Table 6-4 for different lead shield thickness. For this calculation, the photon source 72h after shutdown was used. This means that about 20cm lead shield surrounding the fuel cartridge is required to satisfy the dose rate limit. The radial lead shield would weigh about 32MT for a 3-m long fuel cartridge. Future study should consider minimizing the shield thickness and weight for instance by investigating alternative shield material and optimizing its thickness based on a 3D model of the SPM.

The weight of shielding required for transportation of one Holos SPM will depend on different parameters such as the waiting time between reactor shutdown and SPM transportation, the irradiation history, the average burnup, and the total heavy metal loading. Different optimum Holos concepts displayed in Table 3-5 are expected to show significant variations in shielding weight requirements since the length of the fuel cartridge changes from 2.1m to 4.4m.

Accordingly, detailed shielding analyses will be needed to minimize the shielding requirements for any of these concepts.
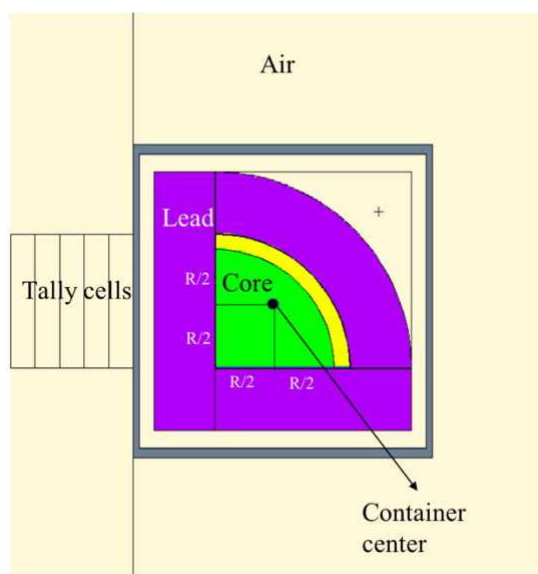

Figure 6-5. Shielding model of 1 SPM during transportation.

Table 6-4. Dose rate for different shield thickness.

Shield thickness (cm)	Dose rate (mrem/hr)	Relative error
50	5.72×10^{-5}	3.51%
30	1.19	1.92%
20	194.50	1.37%

7   Summary and Discussion

The Holos-Quad micro-reactor concept is being proposed by HolosGen for civilian applications to generate 22MWt, using four SPMs fitted into one 40-foot ISO container. It is a very innovative high-temperature gas-cooled reactor concept using TRISO fuel distributed in Graphite hexagonal blocks, cooled with Helium gas. Under ARPA-E MEITNER project initiated in FY2019, the ANL design team has been working on demonstrating the feasibility of the Holos-Quad concept in terms of neutronics and to help advance the core design of the Holos-Quad.

A rigorous design approach was employed for the Holos-Quad in order to ensure the input space is being fully investigated, and that the best solutions are being considered. The first step of this approach consisted of properly defining the Holos-Quad design problem by identifying the competitive design objectives: its economic performance is maximized with longer lifetime and its transportability to remote locations is maximized with reduced weight. The design problem also required to identify the operational constraints (in terms of thermal hydraulics, reactivity feedback and shutdown margins), and the input parameters that could be varied.

In step 2, a sensitivity analysis was performed to enable preliminary investigation of the input space to identify the correlations among input and output variables. It allowed for instance to find input parameters that have relatively poor impact on the core performance and that could be removed from the optimization problem to accelerate its convergence. This sensitivity analysis showed that the design problem defined was highly constrained since only 117 solutions out of 1,000 simulated cores met all the design constraints.

The design optimization was performed in the third step employing a genetic algorithm to effectively explore this highly constrained input space and find global optimal solutions. More than 2,500 cores were fully evaluated to converge to a Pareto Frontier of optimum solutions providing best compromise between the life-time target and the total core weight. The main benefit of this approach was to reduce the human effort and to be able to automatically re-run the optimization problem when changing the design problem. The multi-objective optimization identified various core solutions that would be optimum solutions for different types of applications.

For applications where economics matters less while the focus is on the ease of transportation, a core weight of ~15 tons can achieve lifetime of ~3.5 EFPY. For applications where economics matters the most and ease of transportation matters less, a lifetime of 8.3 equivalent full power years can be achieved with a total core weight of ~26.7 tons. This latter design was determined to be the best configuration that would meet the design requirements of the ARPA-E project and was further investigated with detailed analyses.

In order to give confidence in the neutronic models employed and in the core performance obtained, a detailed neutronic benchmark was proposed based on the selected optimum Holos-Quad core concept. Different engineers at ANL within the Nuclear Science and Engineering (NSE) Division and within the Mathematical Computer and Science (MCS) Division performed independent neutronic evaluations using different Monte Carlo codes (SERPENT and OpenMC) and the PROTEUS deterministic code. The results obtained showed good agreement in the many different evaluated parameters on a unit cell problem and on the full core problem and confirmed the performance of the optimum Holos-Quad concept. Detailed neutronic and thermal-hydraulics were then performed on the optimum core selection in order to provide more details on the power and temperature distributions, to assess the impact from modeling assumptions, and to evaluate

alternative design options. Finally, a very preliminary investigation of secondary control system and shutdown margins was provided.

Shielding analyses were performed by the ARPA-E resource team, and preliminary results are summarized in this report to complete the neutronic feasibility demonstration of this concept. The shielding requirement was assessed for the turbomachinery equipment in the ISO container, which is located near the core. Preliminary results showed that it is important to include ~5cm side shield to prevent the streaming neutrons from reaching the turbine and limit its dose below 0.1 DPA. Another shielding analysis focused on the personnel dose rate outside the reactor building and the thickness of the building wall outside the ISO container was determined from a parametric study. Finally, the shielding requirements during transportation of a single irradiated SPM in an ISO container was evaluated. Preliminary estimation showed 20cm lead shield surrounding the fuel cartridge would be sufficient to satisfy the dose rate limit around the ISO container.

To conclude, the ANL team performed a wide range of extensive analyses in FY2019 to demonstrate the neutronic feasibility of the Holos-Quad micro-reactor concept by proposing an optimum design of the core, thoroughly analyzing it, and performing preliminary shielding analyses. On all these tasks, extensive work is still required to improve some of the economics and neutronics performance. The focus of additional core design optimization will be on reducing the excess reactivity by employing alternative burnable poisons, and on investigating different secondary control systems. A detailed evaluation of shutdown margins for both primary and secondary control systems that include uncertainties and reactivity faults will be completed. Finally, the Holos-Quad design optimization will be updated with higher coolant temperatures (850°C average outlet coolant temperature), steeper limit on the coolant velocity to limit a drop in thermal efficiency, change in location of hafnium blades (directly attached to each SPM), and SiC material considered for coolant sleeves (tolerance to high temperature). It is anticipated that these different changes in core design will help avoiding potential reactivity insertion during flooding scenarios in transportation. Those scenarios will be further evaluated through the core design optimization process.

Finally, the experience and methods developed at ANL within this project for VHTR-types micro-reactor analyses could be directly applicable to advance the design and analyses of additional Holos concepts that are developed for other applications, such as the Titan concept for higher power output and better economic performance, or the SCO FOAK for improved transportability.

REFERENCES

[1] Cost Competitiveness of Micro-Reactors for Remote Markets, NEI, April 15, 2019.

[2] J. Leppanen, "Serpent – a Continuous-energy Monte Carlo Reactor Physics Burnup Calculation Code," User's Manual, June 18, (2015).

[3] P. K. Romano, N. E. Horelik, B. R. Herman, A. G. Nelson, B. Forget, and K. Smith, "OpenMC: A State-of-the-Art Monte Carlo Code for Research and Development," Ann. Nucl. Energy, 82, 90–97 (2015).

[4] Y. S. Jung, C. H. Lee, M. A. Smith, "PROTEUS-MOC User Manual (Rev.0)," ANL/NSE-18/10, Argonne National Laboratory, September 30 (2018).

[5] B. Adams, et al., "Dakota, A Multilevel Parallel Object-Oriented Framework for Design Optimization, Parameter Estimation, Uncertainty Quantification, and Sensitivity Analysis: Version 6.5 User's Manual," Sandia National Laboratory, Albuquerque, NM, U.S.A., 2016.

[6] L. Swiler, et al., "Integration of Dakota into the NEAMS Workbench," Sandia National Laboratories, U.S.A., 2017.

[7] R. Hu, "An advanced one-dimensional finite element model for incompressible thermally expandable flow," Nuclear Technology, Vol. 190, June (2015).

[8] K. Zeng, N. Stauff, J. Hou, T. K. Kim, "Multi-Objectives Core Optimization Study of a Sodium-Cooled Fast Test Reactor" – submitted to Progress in Nuclear Energy, (2019).

[9] J. C. Helton, and F.J. Davis, "Latin hypercube sampling and the propagation of uncertainty in analyses of complex systems." Reliability Engineering and System Safety, Vol. 81, pp. 23-69 (2003).

[10] K. S. Kim, Specification for the VERA Depletion Benchmark Suite. United States: N. p., 2015. Web. doi:10.2172/1256820.

[11] A. E. Craft, Jeffrey C. King, "Reactivity control schemes for fast spectrum space nuclear reactors," *Nuclear Engineering and Design*, Vol. 241, pp 1516–1528, (2011).

[12] C. J. Werner, "MCNP Users Manual - Code Version 6.2", LA-UR-17-29981, Los Alamos National Laboratory (2017).

[13] S. W. Mosher, et al, "ADVANTG – An Automated Variance Reduction Parameter Generator," ORNL/TM-2013/416 Rev. 1, Oak Ridge National Laboratory (2015).

[14] NRC, 10-CFR 71, https://www.nrc.gov/reading-rm/doc-collections/cfr/part071/part071-0047.html.

[15] "Scale: A Comprehensive Modeling and Simulation Suite for Nuclear Safety Analysis and Design," ORNL/TM-2005/39, Version 6.1, June 2011.

[16] B. J. Marsden, *Nuclear graphite for high temperature reactors*. No. IAEA-TECDOC--1238. 2001.

[17] B. J. Marsden, A. Mummery, and P. Mummery. "Modelling the coefficient of thermal expansion in graphite crystals: implications of lattice strain due to irradiation and

pressure." *Proceedings of the Royal Society A: Mathematical, Physical and Engineering Sciences* 474, no. 2218 (2018): 20180075.

[18] C. L. Whitmarsh, *Review of Zircaloy-2 and Zircaloy-4 properties relevant to NS Savannah reactor design*. No. ORNL-3281. Oak Ridge National Lab.(ORNL), Oak Ridge, TN (United States), 1962.

[19] J. A. Phillips, S. G. Nagley, and E. L. Shaber. "Fabrication of uranium oxycarbide kernels and compacts for HTR fuel." *Nuclear Engineering and Design* 251 (2012): 261-281.

[20] D. G. Martin, "The thermal expansion of solid UO2 and (U, Pu) mixed oxides—a review and recommendations." *Journal of Nuclear Materials* 152, no. 2-3 (1988): 94-101.

[21] P. Hidnert and W. T. Sweeney. *Thermal expansion of beryllium and aluminum-beryllium alloys*. No. 565. US Govt. Print. Off., 1927.

[22] R. J. Price, "Thermal conductivity of neutron-irradiated pyrolytic β-silicon carbide." *Journal of Nuclear Materials* 46, no. 3 (1973): 268-272.

[23] W. F. Skerjanc, and B. Collin, "*Assessment of Material Properties for TRISO Fuel Particles used in PARFUME,*" INL/EXT-18-44631, August, 2018.

[24] A. D. Kirshenbaum, J. A. Cahill, and A. V. Grosse. "The density of liquid lead from the melting." *Journal of Inorganic and Nuclear Chemistry* 22, no. 1-2 (1961): 33-38.

[25] S. V. Onufriev, V. A. Petukhov, V. R. Pesochin, and V. D. Tarasov. "The thermophysical properties of hafnium in the temperature range from 293 to 2000 K." *High Temperature* 46, no. 2 (2008): 203-211.

APPENDIX A: MASS DENSITIES OF MATERIALS CONSIDERED

1. Graphite

The density/quality of graphite is limited by fabrication technology. The third generation of nuclear grade graphite can only reach a density of ~1.82 g/cm^3 (at R.T.) due to the existence of porosity. No significant improvement has been made since then [16]. The linear coefficient of thermal expansion (CTE) is around 4×10^{-6} K^{-1} [17]. This gives a density of 1.810 g/cm^3 at 450°C and 1.806 g/cm^3 at 650°C.

2. Helium (at 70 bar or 7 MPa)

As the pressure is not extremely high in this case, the ideal gas equation of state (EOS) can be used.

At 450°C, density is 0.00466 g/cm^3;

At 650°C, density is 0.00365 g/cm^3.

3. Zircaloy-4

Zircaloy-4 density is 6.570 g/cm^3 at 20°C. The thermal expansion in Ref. [18] is as follows (T in °C):

$$L_t = L_0[0.99983 + (5.628 \times 10^{-6})T + (1.581 \times 10^{-9})T^2]$$

Thus, the density at 450°C is 6.517 g/cm^3, while the density at 650°C is 6.489 g/cm^3.

4. UCO

UCO is used to replace UO_2 to mitigate the CO release issue due to UO_2-PyC interaction. The density changes with the fraction of UC_x added. 11.0 g/cm^3 at 20°C is a typical value for UCO kernel density (AGR-2 UCO kernels with 71.4 mole% UO_2, 12.3 mole% $UC_{1.86}$ and 16.4 mole% UC) [19]. Thermal expansion of UO_2 [20] should be used for UCO due to the lack of references.

Thus, the density is 10.861 g/cm^3 at 450°C, 10.794 g/cm^3 at 650°C, and 10.744 g/cm^3 at 800°C.

5. Beryllium [21]

At 20°C, Beryllium density is 1.835 g/cm^3. The linear CTE of beryllium metal from 20°C to 500°C is 15.5×10^{-6} K^{-1}, from 20°C to 700°C is 16.8×10^{-6} K^{-1}. Therefore, the beryllium density is 1.799 g/cm^3 at 450°C and 1.778 g/cm^3 at 650°C.

6. SiC [22]

The density of SiC coating is 3.2 g/cm^3 at 20°C (assuming 99.6% TD). The linear CTE of SiC is 4.9×10^{-6} K^{-1}. At 450°C, the density is 3.180 g/cm^3. At 650°C, the density is 3.171 g/cm^3.

7. Carbon Buffer

A density value of 1.05 g/cm³ is used in PARFUME at 20°C [23]. In the same code, the CTE is (T in °C):

$$\alpha = 5 \times (1 + 0.11 \times \frac{T - 400}{700}) \times 10^{-6}$$

So, the density of carbon buffer is 1.043 g/cm³ at 450°C and 1.040 g/cm³ at 650°C.

8. PyC

PyC density is 1.90 g/cm³ at 20°C in PARFUME [23]. In the same code, the CTE is anisotropic

$$\alpha_r = (30 - 37.5 \times \frac{2}{2 + BAF}) \times (1 + 0.11 \times \frac{T - 400}{700}) \times 10^{-6}$$

$$\alpha_t = (1 + 36 \times \frac{1}{(2 + BAF)^2}) \times (1 + 0.11 \times \frac{T - 400}{700}) \times 10^{-6}$$

Assume a typical BAF (Bacon anisotropic factor) 1.05, the density is 1.888 g/cm³ at 450°C and 1.882 g/cm³ at 650°C.

9. Lead

The density of liquid lead can be found in Ref. [24] (T in K)

$$\rho = 10.678 - 13.174 \times 10^{-4}(T - 600.6)$$

So, the lead density is 10.517 g/cm³ at 450°C and 10.253 g/cm³ at 650°C.

10. Hafnium [25]

The density of hafnium metal is 13.310 g/cm³ at 20°C. The density of Hf is 13.203 g/cm³ at 450°C and 13.145 g/cm³ at 650°C.

APPENDIX B: MODEL DEVELOPED WITH PROTEUS

B.1 Geometry and Mesh Generation for PROTEUS

Geometry and mesh of Holos benchmark cores for PROTEUS were generated using CUBIT and the in-house mesh toolkit. 2D meshes were generated to solve 2D and 3D core problems with PROTEUS-MOC, which solves problems based on the extruded geometry. Since the Holos core is based on a non-standard geometry requiring a significant effort to deal with a whole-core geometry and mesh using CUBIT, we generated meshes for core components such as fuel assemblies and out-core regions using CUBIT and merged them using the in-house mesh toolkit to construct a whole core. This allowed us to save time and effort in generating geometries and meshes.

Figure B-1 shows the unit cell benchmark problems, among which configuration B (pitch = 1.7*2 cm) was selected for comparison with Monte Carlo (SERPENT and OpenMC) solutions even though configuration A (pitch = 1.7*√3 cm) was more closely representing a unit cell of the fuel region of the core. Meshes were generated using CUBIT.

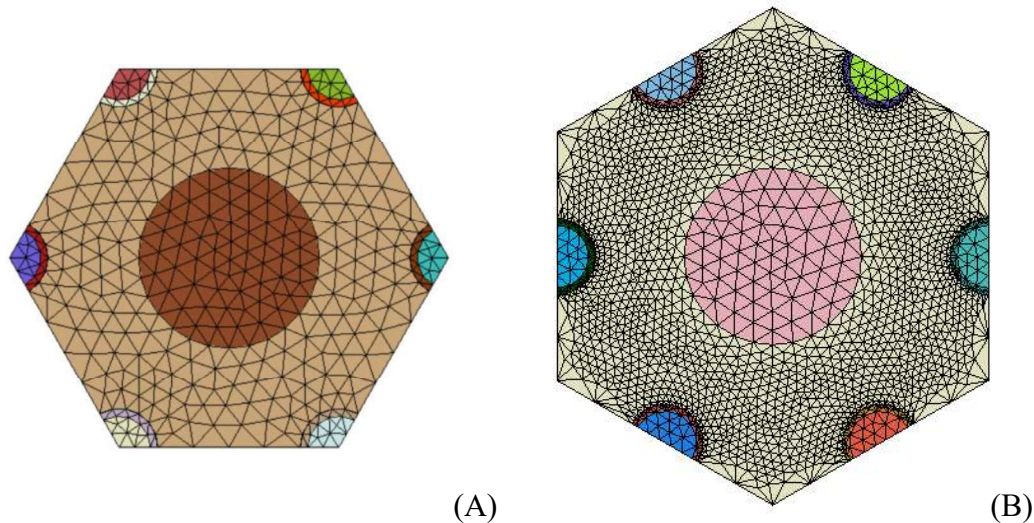(A)   (B)

Figure B-1. Unit cell benchmark problems.

In order to contruct a whole core geometry and mesh, at first set of assembly meshes were generated using CUBIT. Since the core is composed of partial fuel assemblies along the SPM boundaries as well as whole fuel assemblies, we generated geometry and mesh for partial fuel assemblies shown in Figure B-2 as well. Those four types were used to construct the core composed of fuel assemblies only, by merging fuel assemblies using the in-house mesh toolkit. The resulting geometry is shown in Figure B-2 (bottom left).

Geometry and mesh were generated for out-cores with different SPM conditions in the ISO container (no separation, full separation, and full separation with the control blade), as shown in Figure B-3. A quarter core is constructed by merging the core and out-core components using the in-house mesh toolkit. Four quarter cores are merged to make a whole core. A whole core with asymmetric SPM separations, 3 SPM separation for example, is generated by merging 3 quarter cores with SPM separation and 1 quarter core with no SPM separation.
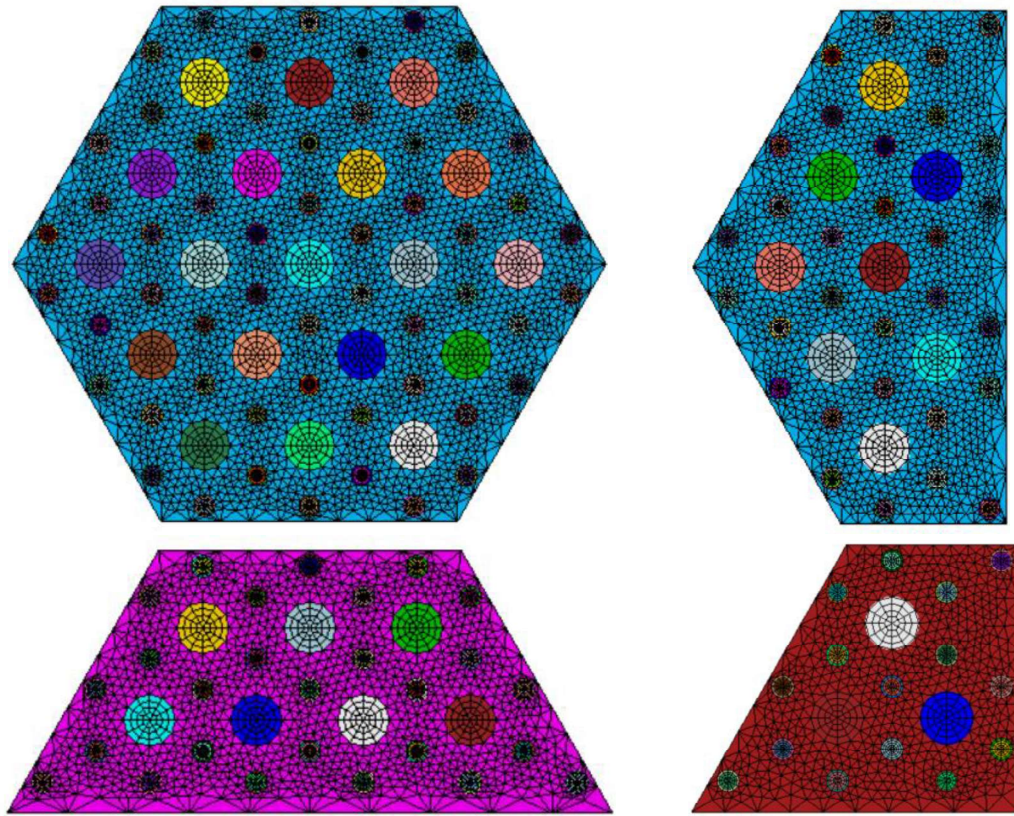
Figure B-2. Fuel assembly meshes generated from CUBIT.

Part of the detailed meshes of a whole core are illustrated in Figure B-4. As seen in the figure, meshes should be conformal between different material regions since PROTEUS does not handle non-conformal meshes. Both quad and triangle meshes were used. In particular, the meshed areas for fuel and coolant regions were slightly adjusted to preserve those of the actual regions.

Boundary surfaces (curves) for boundary conditions are specified using sidesets, and regions are defined as blocks with names such that materials and cross sections are assigned to regions for PROTEUS calculations. The PROTEUS core model obtained is shown in Figure B-5.
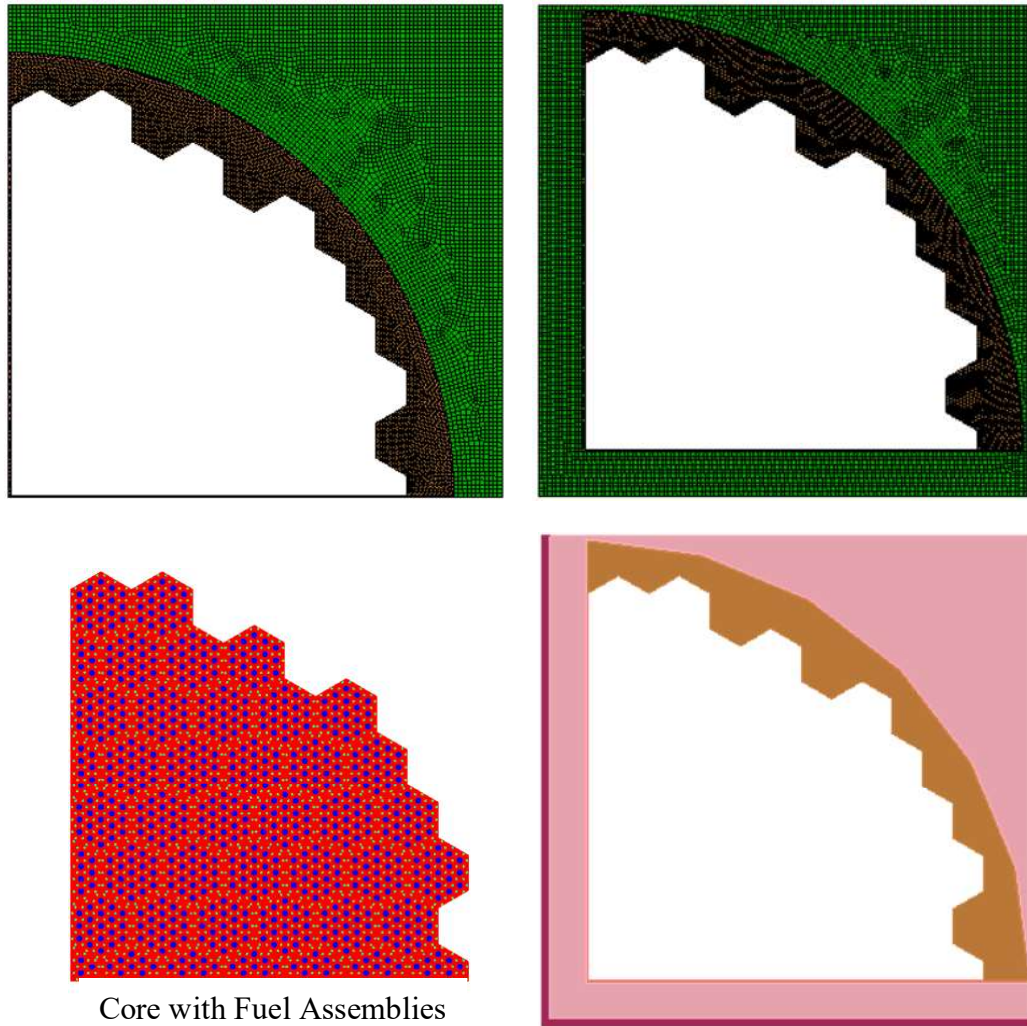
Core with Fuel Assemblies

Figure B-3. Core and out-core meshes generated with CUBIT.
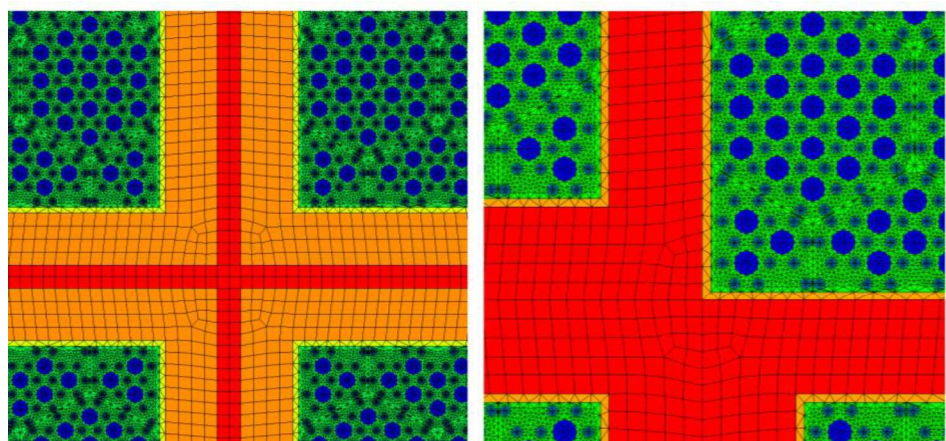
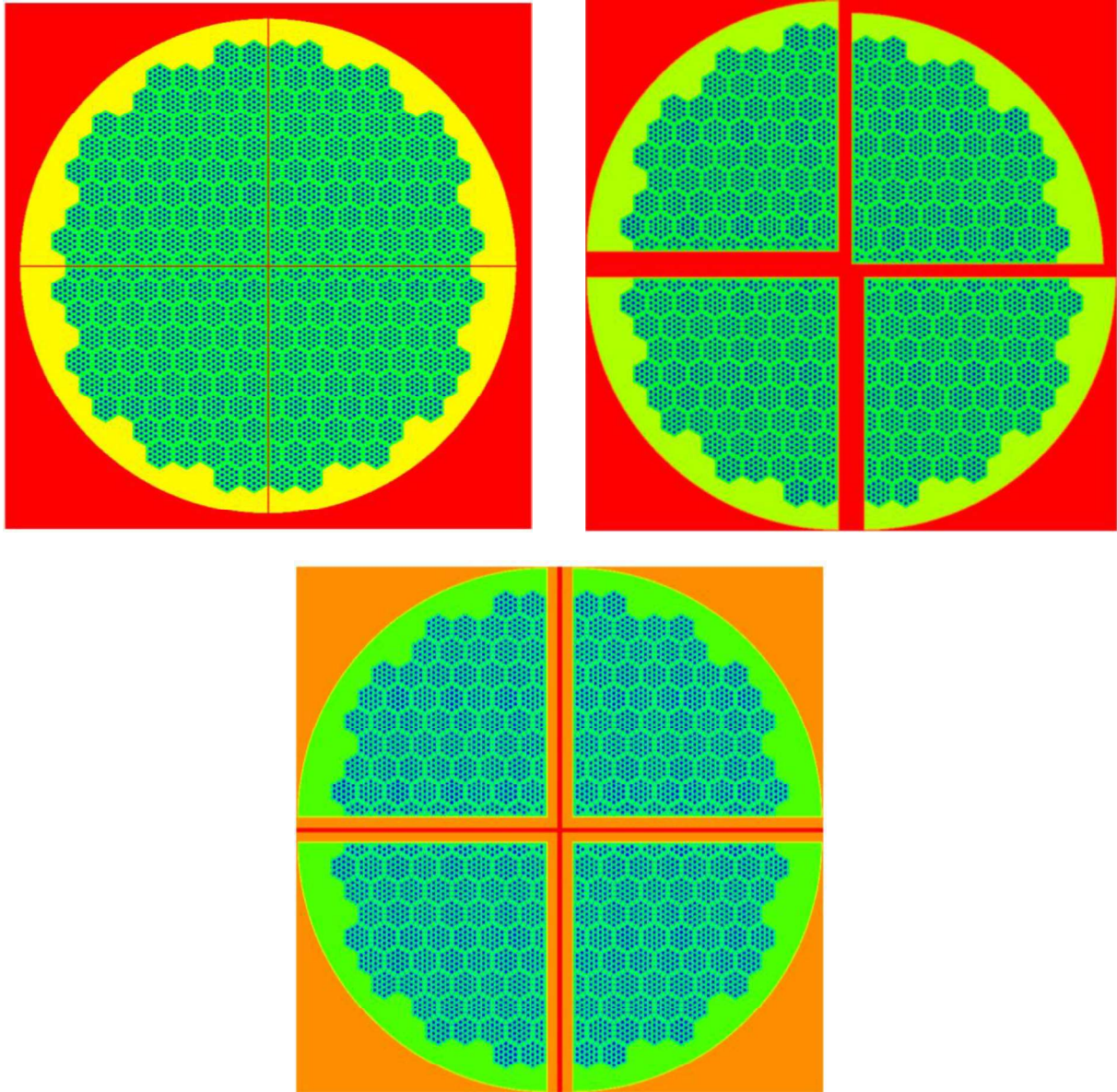

Figure B-4. Details of core meshes.

Figure B-5. PROTEUS core models with different SPM configurations.

B.2 Cross sections for PROTEUS

Cross sections were generated using SERPENT / GenISOTXS. The 2D core without gap between SPMs was calculated using SERPENT, and multi-group cross sections are extracted from SERPENT outputs using GenISOTXS. Multigroup cross sections would be different from regions even with the same composition because of different self-shielding effects, but we produced one representative set of cross sections for each region (i.e., fuel, coolant, graphite, reflector, control blade, and shell).

The double heterogeneity effect due to TRISO particles was dealt with by SERPENT, not directly by PROTEUS. The 14-group cross sections based on the group structure listed in Table B-1 were extracted. The neutron flux spectra for the Holos cores with different configurations are

illustrated in Figure 5-1. The neutron flux spectra for calculations 1, 2, 5, and 6 are similar to each other, which are typical neutron flux spectra for cores with graphite moderator. Calculation 3 in which 4 SPMs are fully separated and the Hf control blade is fully inserted at the center shows relatively a smaller amount of thermal cross sections due to the neutron absorption of the Hf control blade. Calculation 4 in which all holes are filled with water in addition to the calculation 3 condition shows a larger amount of thermal cross sections due to the neutron thermalization in water. Since the neutron flux spectra are very different between calculations 1, 2, 5, 6, calculation 3, and calculation 4, a relatively good number of energy groups would be necessary to cover the wide range of neutron spectrum. In these benchmark calculations, we used 14 group cross sections generated from SERPENT for each calculation.

Table B-1. 14 Group structure (upper energies).

G	Energy (eV)	G	Energy (eV)	G	Energy (eV)	G	Energy (eV)
1	2.00000e+06	2	1.35300e+06	3	5.00000e+05	4	9.11800e+03
5	3.67260e+02	6	4.00000e-00	7	1.50000e-00	8	5.00000e-01
9	4.00000e-01	10	3.00000e-01	11	2.50000e-01	12	1.80000e-01
13	1.00000e-01	14	5.00000e-02				

B.2 PROTEUS Solutions for 2D and 3D Cores

2D and 3D cores with different SPM conditions and different materials in the gap between SPMs were calculated with PROTEUS. For 2D cores, 332,449 elements, 80 angles (L3T9) or 128 angles (L3T15) per all directions, 14 groups were used, while for 3D cores with 400 cm high including 390 cm fuel region with 5 cm top and bottom axial reflectors, 21 axial planes per a half core were used.

Table B-2 shows comparison of eigenvalues for the 2D calculations between SERPENT and PROTEUS. All eigenvalues are in good agreement between the two code solutions, except for calculations 3 and 4 in which the Hf control blade is inserted. It was indicated that the MDC and FTC agree very well between SERPENT and PROTEUS. As a future work, further investigation would be necessary to figure out the sources of the difference observed in the calculations with Hf control blade.

Table B-2.Benchmark results comparison for 2D core problems.

Calc #	Description	SERPENT	PROTEUS (*Δk)
1	Reference K-eff	1.08191 ± 0.00014	1.08021 (-170)
2	Reactivity worth at hot shutdown of moving 3 SPMs out of 4, with maximum gap thickness of 21cm	0.96731 ± 0.00017	0.96557 (-174)
3	Shutdown margins at cold shutdown with maximum gap thickness of 21cm between each of the 4 SPMs, and insertion of Hafnium blade	0.82282 ± 0.00017	0.81645 (-637)
4	Water flooding at cold shutdown (described in #3) with water (1g/cm^3, 300K) in coolant holes and outside SPMs.	1.05583 ± 0.00022	1.04864 (-719)
5	Moderator density coefficient with reduced graphite density of the fuel pin matrix and the graphite block by 1%	1.08008 ± 0.00014	1.07732 (-276)
6	Doppler coefficient calculated by increasing the temperature of the UCO fuel by 300K	1.07040 ± 0.00015	1.06880 (-160)
	MDC = 1e5*(1/#1 - 1/#5)	-16	-25
	FTC = 1e5*(1/#1 - 1/#6)	-99	-99

* Δk : eigenvalue difference from SERPENT, pcm

Figure B-6 and Figure B-7 illustrate 2D thermal (0.1 – 0.2 eV) and fast (0.9 keV – 0.5 MeV) neutron flux distributions for calculation 2 (3 SPM separation), calculation 3 (SPM separation with Hf control blade) and calculation 4 (calculation 3 + flooded), produced from PROTEUS. As seen in the figures, large thermal fluxes are shown in the reflector region, and when flooded more thermalization was made in the center region filled with water.

3D thermal and fast neutron flux distributions for calculations 1 and 2 produced from PROTEUS are discussed in Section 5.1.
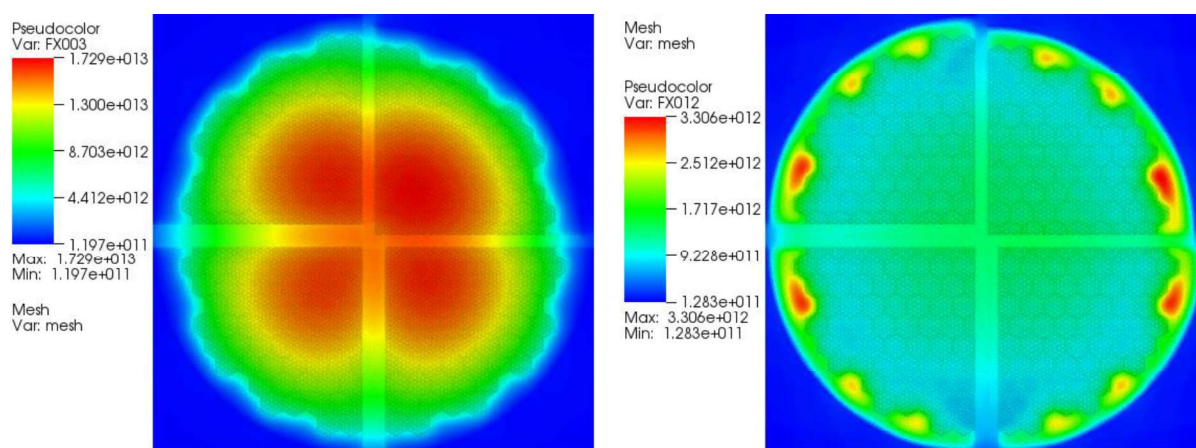
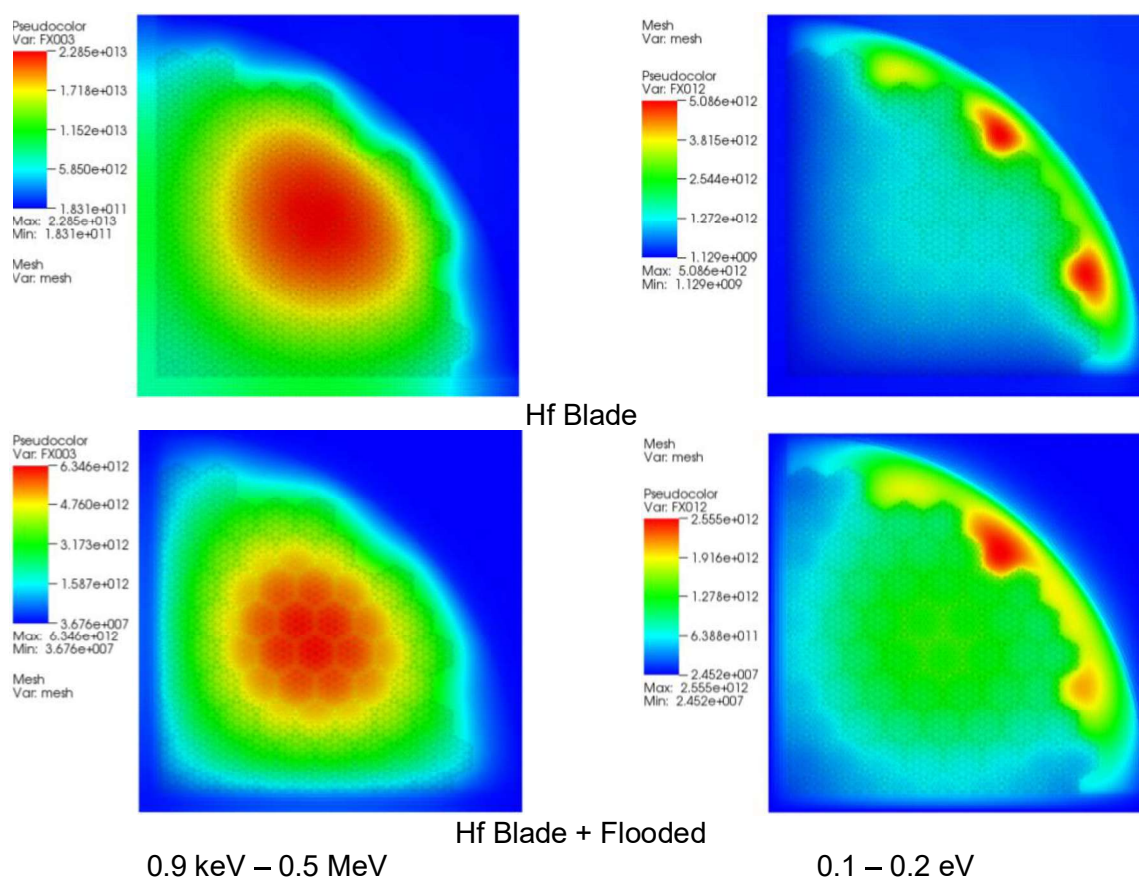Figure B-6. Thermal and fast flux distributions of 2D Holos cores for calculation 2.

Hf Blade

Hf Blade + Flooded

0.9 keV – 0.5 MeV   0.1 – 0.2 eV

Figure B-7. Thermal and fast flux distributions of 2D Holos cores for calculations 3 and 4.

Nuclear Science and Engineering Division
Argonne National Laboratory
9700 South Cass Avenue, Bldg. 208
Argonne, IL 60439

www.anl.gov